Michael Raba: Mechanical Engineering Portfolio 2025

Abstract

This book is a compilation of projects of Michael Raba and can be found at:
https://michaelraba.github.io/talks/

Table of Contents

Anand Model: Viscoelastoplasticity

Michael Raba, MSc Candida

Created: 2025-0

and its Application to Solder Joints

te at University of Kentucky

4-29 Tue 06:39

Constitutive Equations for Hot-Working of Metals

Author: Lallit Anand (1985)

DOI: 10.1016/0749-6419(85)90004-X

One of the foundational papers in thermodynamically consistent viscoplasticity modeling—especially significant in the context of metals subjected to large strains and high temperatures.

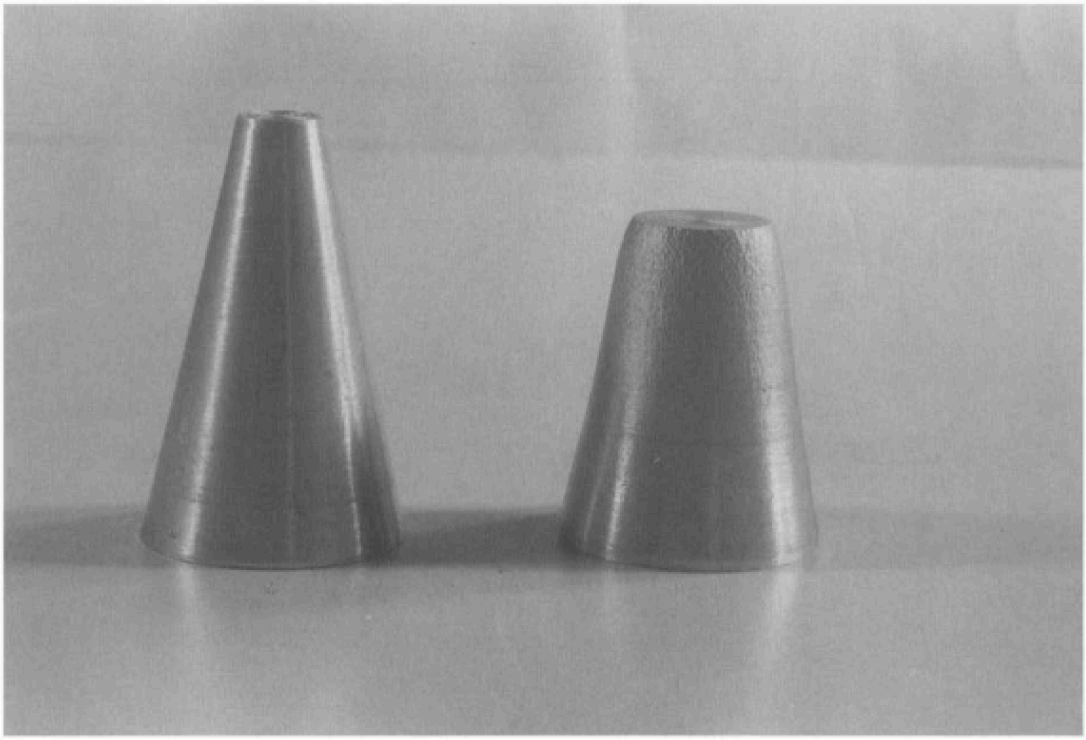

Fig. 25. 1100 aluminum state gradient specimens before and after testing.

e Paper

International Journal of Plasticity, Vol. 1, pp. 213–231, 1985
Printed in the U.S.A.

0749-6419/85 $3.00 + .00

CONSTITUTIVE EQUATIONS FOR HOT-WORKING OF METALS

LALLIT ANAND

Massachusetts Institute of Technology

(Communicated by Theoder Lehmann, Ruhr Universität Bochum)

Abstract—Elevated temperature deformation processing—"hot-working," is an important step during the manufacturing of most metal products. Central to any successful analysis of a hot-working process is the use of appropriate rate and temperature-dependent constitutive equations for large, interrupted inelastic deformations, which can faithfully account for strain-hardening, the restoration processes of recovery and recrystallization and strain rate and temperature history effects. In this paper we develop a set of phenomenological, internal variable type constitutive equations describing the elevated temperature deformation of metals. We use a scalar and a symmetric, traceless, second-order tensor as internal variables which, in an average sense, represent an isotropic and an anisotropic resistance to plastic flow offered by the internal state of the material. In this theory, we consider small elastic stretches but large plastic deformations (within the limits of texturing) of isotropic materials. Special cases (within the constitutive framework developed here) which should be suitable for analyzing hot-working processes are indicated.

I. INTRODUCTION

Hot-working is an important processing step during the manufacture of approximately more than eighty-five percent of all metal products. The main features of hot-working are that metals are deformed into the desired shapes at temperatures in the range of ~ 0.5 through $\sim 0.9\ \theta_m$, where θ_m is the melting temperature in degrees Kelvin, and at strain rates in the range of $\sim 10^{-4}$ through $\sim 10^{3}$/sec. It is to be noted that most hot-working processes are more than mere shape-making operations; an important goal of hot-working is to subject the workpiece to appropriate thermo-mechanical processing histories which will produce microstructures that optimize the mechanical properties of the product.

The major quantities of metals and alloys are hot-worked under interrupted non-isothermal conditions. The principles of the physical metallurgy of such deformation processing are now well recognized, e.g., JONAS *et al.* [1969], SELLARS & MCG TEGART [1972], MCQUEEN & JONAS [1975], and SELLARS [1978]. During a deformation pass, the stress is found to be a strong function of the strain rate, temperature, and the defect and microstructural state of the material. The strain-hardening produced by the deformation tends to be counteracted by dynamic recovery processes. These recovery processes result in a rearrangement and annihilation of dislocations in such a manner that as the strain in a pass increases, the dislocations tend to arrange themselves into subgrain walls. In some metals and alloys (especially those with a high stacking fault energy, e.g., Al, α-Fe and other ferritic alloys) dynamic recovery can balance strain-hardening and an apparent steady state stress level can be achieved and maintained to large strains before fracture occurs. In other metals and alloys in which recovery is less rapid (especially those metals with low stacking fault energies, e.g., Ni, γ-Fe and other austenitic

Case Study: Wang (2

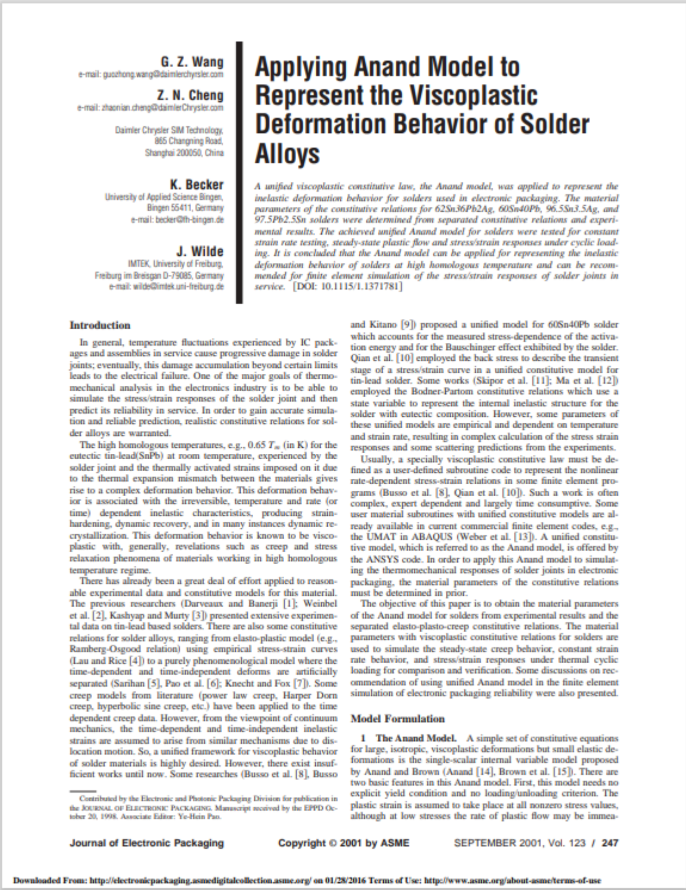

G. Z. Wang
e-mail: guozhong.wang@daimlerchyrsler.com

Z. N. Cheng
e-mail: zhaonian.cheng@daimlerChrysler.com

Daimler Chrysler SIM Technology,
865 Changning Road,
Shanghai 200050, China

K. Becker
University of Applied Science Bingen,
Bingen 55411, Germany
e-mail: becker@fh-bingen.de

J. Wilde
IMTEK, University of Freiburg,
Freiburg im Breisgan D-79085, Germany
e-mail: wilde@imtek.uni-freiburg.de

Applying Anand Model to Represent the Viscoplastic Deformation Behavior of Solder Alloys

A unified viscoplastic constitutive law, the Anand model, was applied to represent the inelastic deformation behavior for solders used in electronic packaging. The material parameters of the constitutive relations for 62Sn36Pb2Ag, 60Sn40Pb, 96.5Sn3.5Ag, and 97.5Pb2.5Sn solders were determined from separated constitutive relations and experimental results. The achieved unified Anand model for solders were tested for constant strain rate testing, steady-state plastic flow and stress/strain responses under cyclic loading. It is concluded that the Anand model can be applied for representing the inelastic deformation behavior of solders at high homologous temperature and can be recommended for finite element simulation of the stress/strain responses of solder joints in service. [DOI: 10.1115/1.1371781]

Introduction

In general, temperature fluctuations experienced by IC packages and assemblies in service cause progressive damage in solder joints; eventually, this damage accumulation beyond certain limits leads to the electrical failure. One of the major goals of thermo-mechanical analysis in the electronics industry is to be able to simulate the stress/strain responses of the solder joint and then predict its reliability in service. In order to gain accurate simulation and reliable prediction, realistic constitutive relations for solder alloys are warranted.

The high homologous temperatures, e.g., 0.65 T_m (in K) for the eutectic tin-lead(SnPb) at room temperature, experienced by the solder joint and the thermally activated strains imposed on it due to the thermal expansion mismatch between the materials gives rise to a complex deformation behavior. This deformation behavior is associated with the irreversible, temperature and rate (or time) dependent inelastic characteristics, producing strain-hardening, dynamic recovery, and in many instances dynamic recrystallization. This deformation behavior is known to be viscoplastic with, generally, revelations such as creep and stress relaxation phenomena of materials working in high homologous temperature regime.

There has already been a great deal of effort applied to reasonable experimental data and constitutive models for this material. The previous researchers (Darveaux and Banerji [1]; Weinbel et al. [2], Kashyap and Murty [3]) presented extensive experimental data on tin-lead based solders. There are also some constitutive relations for solder alloys, ranging from elasto-plastic model (e.g., Ramberg-Osgood relation) using empirical stress-strain curves (Lau and Rice [4]) to a purely phenomenological model where the time-dependent and time-independent deforms are artificially separated (Sarihan [5], Pao et al. [6]; Knecht and Fox [7]). Some creep models from literature (power law creep, Harper Dorn creep, hyperbolic sine creep, etc.) have been applied to the time dependent creep data. However, from the viewpoint of continuum mechanics, the time-dependent and time-independent inelastic strains are assumed to arise from similar mechanisms due to dislocation motion. So, a unified framework for viscoplastic behavior of solder materials is highly desired. However, there exist insufficient works until now. Some researches (Busso et al. [8], Busso and Kitano [9]) proposed a unified model for 60Sn40Pb solder which accounts for the measured stress-dependence of the activation energy and for the Bauschinger effect exhibited by the solder. Qian et al. [10] employed the back stress to describe the transient stage of a stress/strain curve in a unified constitutive model for tin-lead solder. Some works (Skipor et al. [11]; Ma et al. [12]) employed the Bodner-Partom constitutive relations which use a state variable to represent the internal inelastic structure for the solder with eutectic composition. However, some parameters of these unified models are empirical and dependent on temperature and strain rate, resulting in complex calculation of the stress strain responses and some scattering predictions from the experiments.

Usually, a specially viscoplastic constitutive law must be defined as a user-defined subroutine code to represent the nonlinear rate-dependent stress-strain relations in some finite element programs (Busso et al. [8], Qian et al. [10]). Such a work is often complex, expert dependent and largely time consumptive. Some user material subroutines with unified constitutive models are already available in current commercial finite element codes, e.g., the UMAT in ABAQUS (Weber et al. [13]). A unified constitutive model, which is referred to as the Anand model, is offered by the ANSYS code. In order to apply this Anand model to simulating the thermomechanical responses of solder joints in electronic packaging, the material parameters of the constitutive relations must be determined in prior.

The objective of this paper is to obtain the material parameters of the Anand model for solders from experimental results and the separated elasto-plasto-creep constitutive relations. The material parameters with viscoplastic constitutive relations for solders are used to simulate the steady-state creep behavior, constant strain rate behavior, and stress/strain responses under thermal cyclic loading for comparison and verification. Some discussions on recommendation of using unified Anand model in the finite element simulation of electronic packaging reliability were also presented.

Model Formulation

1 The Anand Model. A simple set of constitutive equations for large, isotropic, viscoplastic deformations but small elastic deformations is the single-scalar internal variable model proposed by Anand and Brown (Anand [14], Brown et al. [15]). There are two basic features in this Anand model. First, this model needs no explicit yield condition and no loading/unloading criterion. The plastic strain is assumed to take place at all nonzero stress values, although at low stresses the rate of plastic flow may be immea-

Contributed by the Electronic and Photonic Packaging Division for publication in the JOURNAL OF ELECTRONIC PACKAGING. Manuscript received by the EPPD October 20, 1998. Associate Editor: Ye-Hein Pao.

Source: Wang, C. H. (2001). "A Unified Creep–Plasticity Model for Solder Alloys."
DOI: 10.1115/1.1371781

- Applies An
- Anand's m
- transition t
- Targets so
connectior

001) Apply to Solder

Why Wang's Paper Matters

and's unified viscoplastic framework to model solder behavior.
odel can be reduced and fitted from experiments.
he theory into engineering-scale implementation.
lder joints in microelectronic packages (chip on PCB, soldered
ns).

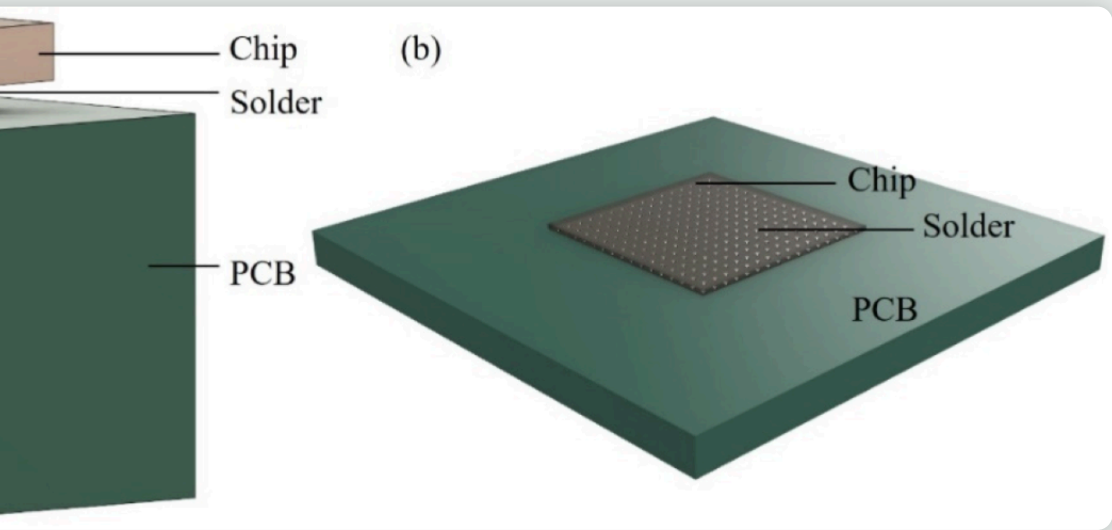

Observed Behavior

- **Top Graph (a):** $\dot{\varepsilon} = 10^{-2}\,\mathrm{s}^{-1}$
- High strain rate → higher stress
- Recovery negligible → pronounced hardening
- **Bottom Graph (b):** $\dot{\varepsilon} = 10^{-4}\,\mathrm{s}^{-1}$
- Lower strain rate → lower stress at same strain
- Recovery and creep effects more significant

Model Accuracy: Lines = model prediction, X = experimental data

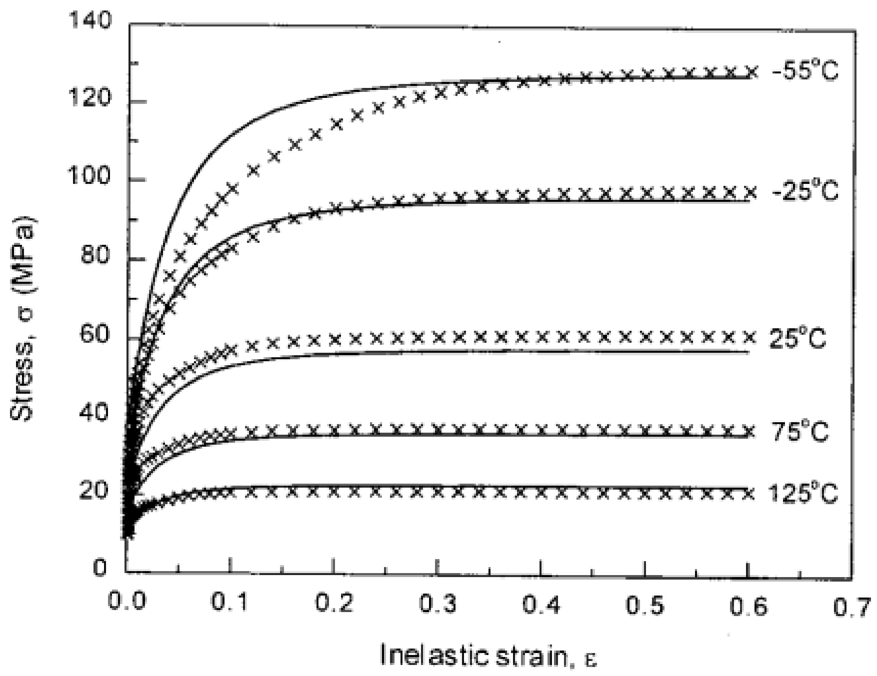

(a) $\dot{\varepsilon} = 1.0\times10^{-2}\ \mathrm{s}^{-1}$

Key Insights from Wang (2001)

- "At lower strain rates, recovery dominates… the stress levels off early."
- "At high strain rates, hardening dominates, and the stress grows continuously."

Anand's model smoothly captures strain-rate and temperature dependence of solder materials.

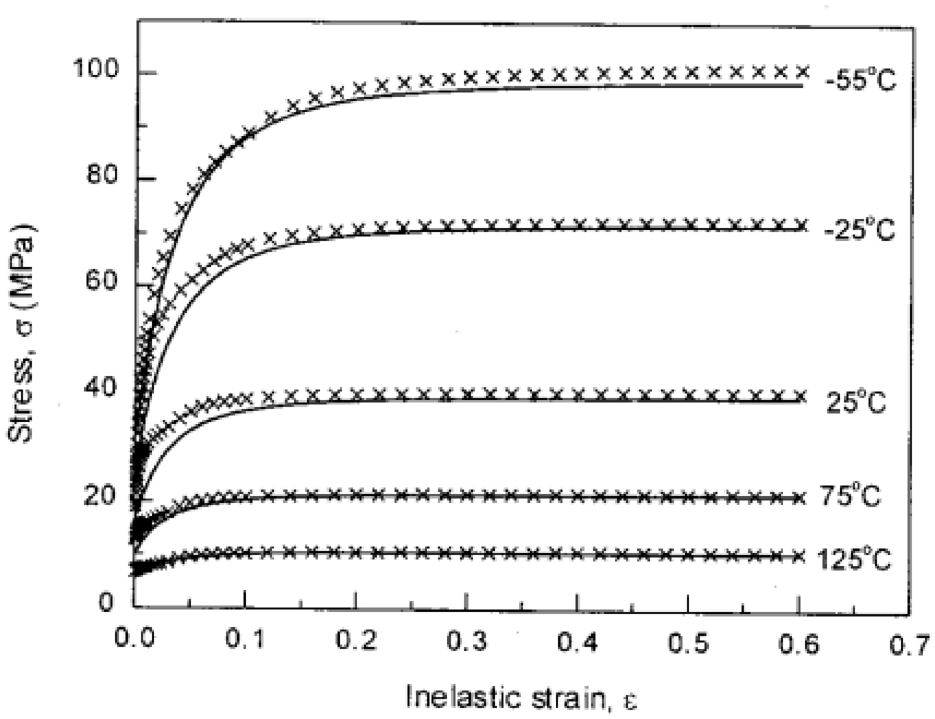

(b) $\dot{\varepsilon}=1.0\times10^{-4}\ s^{-1}$

Flow Rule (Plastic Strain Rate)

- $$\dot{\varepsilon}^p = A \exp\left(-\frac{Q}{RT}\right)\left[\sinh\left(\frac{j\sigma}{s}\right)\right]^{1/m}$$
- Plastic strain rate increases with stress and temperature.
- No explicit yield surface; flow occurs at all nonzero stresses.

Deformation Resistance Saturation s^*

- $$s^* = \hat{s}\left(\frac{\dot{\varepsilon}^p}{A}\exp\left(\frac{Q}{RT}\right)\right)^n$$
- Defines the steady-state value that s evolves toward.
- Depends on strain rate and temperature.

and-Type Viscoplastic Model

Evolution of Deformation Resistance s

- $$\dot{s} = h_0 \left| 1 - \frac{s}{s^*} \right|^a \operatorname{sign}\left(1 - \frac{s}{s^*}\right) \dot{\varepsilon}^p$$
- Describes dynamic hardening and softening of the material.
- s evolves depending on proximity to s^* and flow activity.

Note: Constants $A, Q, m, j, h_0, \hat{s}, n, a$ are material-specific and fitted to experimental creep/strain rate data.

Image Reference

Values are from correspond to 60Sn40Pb solder parameters used in Anand's model:

- S_0: Initial deformation resistance
- Q/R: Activation energy over gas constant
- A: Pre-exponential factor for flow rate
- ξ: Multiplier of stress inside sinh
- m: Strain rate sensitivity of stress
- h_0: Hardening/softening constant
- $\hat{s}$: Coefficient for saturation stress
- n: Strain rate sensitivity of saturation
- a: Strain rate sensitivity of hardening or softening

Constants for 60Sn40Pb

Numerical Values

- $S_0 = 5.633 \times 10^7$ Pa
- $Q/R = 10830$ K
- $A = 1.49 \times 10^7$ s^{-1}
- $\xi = 11$
- $m = 0.303$
- $h_0 = 2.6408 \times 10^9$ Pa
- $\hat{s} = 8.042 \times 10^7$ Pa
- $n = 0.0231$
- $a = 1.34$

These constants match Wang's paper for modeling 60Sn40Pb viscoplasticity.

Initialization

- Material constants: $A, Q/R, j, m, h_0, \hat{s}, n, a, E$
- Strain rate: $\dot{\varepsilon}$
- Temperature set: $\{T_i\}$
- Set: $\varepsilon^p(0) = 0, \quad s(0) = \hat{s}$

Time Evolution Loop

1. $\varepsilon_{\text{total}}(t) = \dot{\varepsilon} t$
2. $\sigma_{\text{trial}} = E(\varepsilon_{\text{total}} - \varepsilon^p)$
3. Compute $x = \frac{j\sigma}{s}$
4. Approximate $\sinh(x)$ (linearize if $|x| \ll 1$)
5. $\dot{\varepsilon}^p = Ae^{-Q/RT}(\sinh(x))^{1/m}$

ntegration scheme Pseudocode

Plastic Flow & Resistance Evolution

6. $s^* = \hat{s}\left(\frac{\dot{\varepsilon}^p}{A} e^{Q/RT}\right)^n$
7. $\dot{s} = h_0 \left|1 - \frac{s}{s^*}\right|^a \mathrm{sign}\left(1 - \frac{s}{s^*}\right) \dot{\varepsilon}^p$
8. Update: $\varepsilon^p(t + \Delta t) = \varepsilon^p(t) + \dot{\varepsilon}^p \Delta t$
9. Update: $s(t + \Delta t) = s(t) + \dot{s}\Delta t$
10. Record $(\varepsilon_{\text{total}}, \sigma_{\text{trial}})$

Termination

- Stop when $\varepsilon_{\text{total}} \geq \varepsilon_{\max}$
- Plot σ vs ε for all T_i

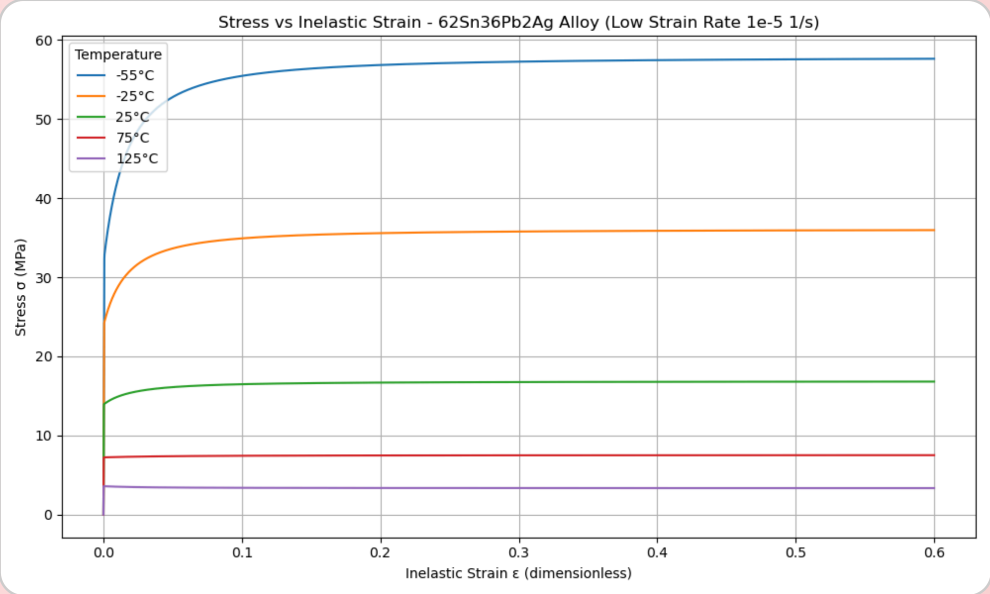

Forward Euler Scher

```
import numpy as np
import matplotlib.pyplot as plt
from scipy.integrate import solve_ivp

# Material constants for 62Sn36Pb2Ag solder alloy
A = 2.24e8       # 1/s
Q_R = 11200      # K
j = 13           # dimensionless
m = 0.21         # dimensionless
h0 = 1.62e10     # Pa
s0 = 8.47e7      # Pa
s_hat = 8.47e7   # Pa
n = 0.0277       # dimensionless
a = 1.7          # dimensionless
E = 5.2e10       # Pa (Elastic modulus)

# Temperatures in Kelvin
T_C = [-55, -25, 25, 75, 125]
T_list = [T + 273.15 for T in T_C]

# Simulation parameters
strain_rate = 1e-5  # 1/s
eps_total_max = 0.6
t_max = eps_total_max / strain_rate
time_steps = 10000
t_eval = np.linspace(0, t_max, time_steps)

# Define the ODE system
def system(t, y, T):
    ep_p, s = y
    eps_total = strain_rate * t
    sigma_trial = E * (eps_total - ep_p)
    x = j * sigma_trial / s

    if np.abs(x) < 0.01:
        sinh_x = x
    else:
        sinh_x = np.sinh(np.clip(x, -30, 30))

    sinh_x = np.maximum(sinh_x, 1e-12)
    dep_p = A * np.exp(-Q_R / T) * sinh_x**(1/m)

    s_star = s_hat * (dep_p / A * np.exp(Q_R / T))**n
    ds = h0 * np.abs(1 - s/s_star)**a * np.sign(1 - s/s_star) * dep_p

    return [dep_p, ds]

# Plotting
```

me for Anand Model

Strain rate sensit

- As $m \to 0$, rate insensitive
- As $m \to 1$, small stress ch

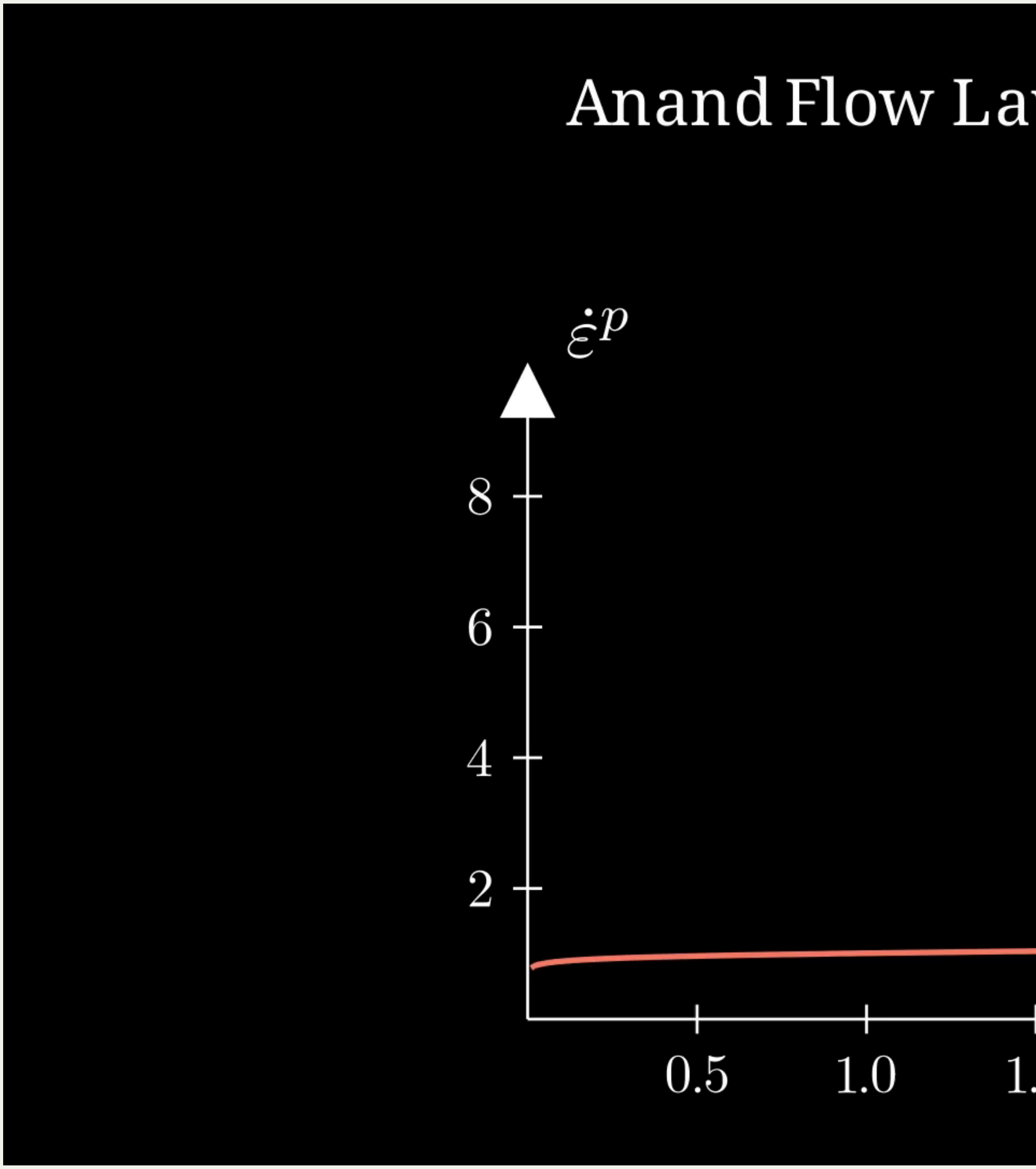

tivity of stress m

e (yield)
ange causes big change in strain rate

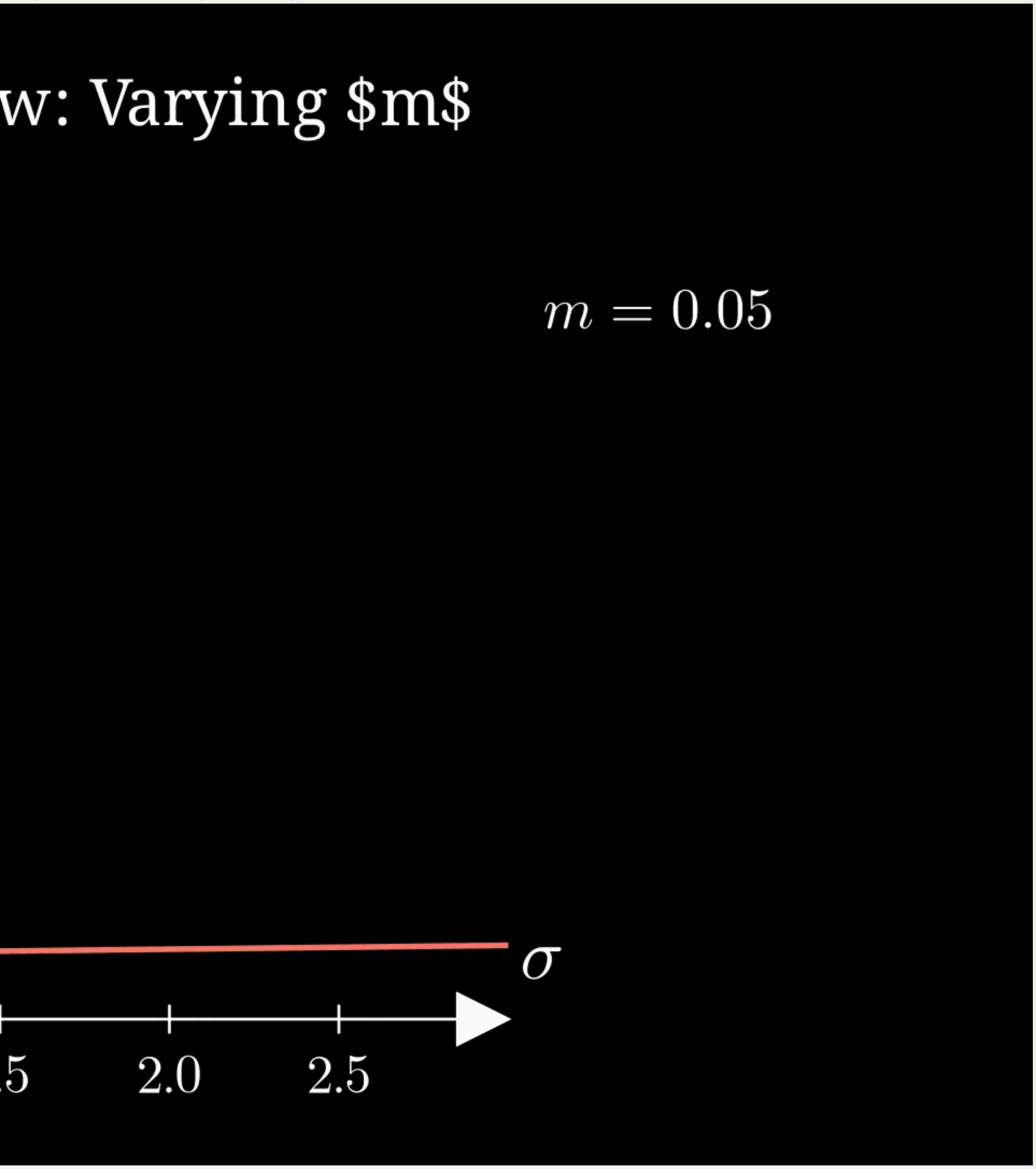

Tensorial Flow Rule (directional form)

$$\mathbf{D}^p = \dot{\epsilon}^p \left(\frac{3}{2} \frac{\mathbf{T}'}{\bar{\sigma}} \right)$$

Equivalent Stress Definition

$$\bar{\sigma} = \sqrt{\frac{3}{2}\mathbf{T}' : \mathbf{T}'}$$

Summary:

- Direction given by $\mathbf{T}'$.
- Magnitude determined by hyperbolic
- $\bar{\tau}$ represents the effective shear stre
- $\bar{\sigma} = \sqrt{\frac{3}{2}\mathbf{T}' : \mathbf{T}'}$ is the von Mises Eq
- Full flow = **direction** × **magnitude**.

r rule

Plastic Strain Rate (magnitude form)

$$\dot{\epsilon}^p = A \exp\left(-\frac{Q}{R\theta}\right)\left[\sinh\left(\xi\frac{\bar{\sigma}}{s}\right)\right]^{1/m}$$

Full Flow Rule with Hyperbolic Sine

$$\mathbf{D}^p = A \exp\left(-\frac{Q}{R\theta}\right)\left[\sinh\left(\xi\frac{\bar{\sigma}}{s}\right)\right]^{1/m}\left(\frac{3}{2}\frac{\mathbf{T}'}{\bar{\sigma}}\right),$$

$$= \dot{\gamma}^p\left(\frac{\widetilde{\mathbf{T}}'}{2\bar{\tau}}\right), \quad \bar{\tau} = \left\{\frac{1}{2}\mathrm{tr}(\widetilde{\mathbf{T}}'^2)\right\}^{1/2}$$

c sine based on $\bar{\sigma}/s$.
ess computed from deviatoric stress.
uivalent stress, but is formally defined without yield point

Stress Evolution Equation (Rate form of Hooke's Law)

$$\overset{\nabla}{\mathbf{T}} = \mathbb{L}\left[\mathbf{D} - \mathbf{D}^p\right] - \mathbf{\Pi}\dot{\theta}$$

(rate-form Hooke’s law for finite deformation plasticity, with frame-indifference enforced through the Jaumann rate.)

Jaumann Rate Definition

$$\overset{\nabla}{\mathbf{T}} = \dot{\mathbf{T}} - \mathbf{W}\mathbf{T} + \mathbf{T}\mathbf{W}$$

Summary:

- Stress rate follows Jaum
- Elastic response govern
- Thermal expansion intro

ion for the Stress

Material Tensors and Operators

- $\mathbb{L} = 2\mu\mathbf{I} + \left(\kappa - \frac{2}{3}\mu\right)\mathbf{1}\otimes\mathbf{1}$ — isotropic elasticity tensor
- $\mathbb{L}\mathbf{D}$ represents how instantaneous strain rates generate stresses according to the elastic material's stiffness properties.
- $\mu = \mu(\theta)$, $\kappa = \kappa(\theta)$ — temperature-dependent moduli
- $\mathbf{\Pi} = (3\alpha\kappa)\mathbf{1}$ — stress-temperature coupling
- $\alpha = \alpha(\theta)$ — thermal expansion coefficient
- $\mathbf{D} = \mathrm{sym}(\nabla\mathbf{v})$ — stretching tensor
- $\mathbf{W} = \mathrm{skew}(\nabla\mathbf{v})$ — spin tensor
- $\mathbf{I}$ = fourth-order identity tensor
- $\mathbf{1}$ = second-order identity tensor

---

nann derivative to ensure frame indifference.
ned by isotropic fourth-order tensor $\mathbb{L}$.
oduces additional stress through $\mathbf{\Pi}\dot{\theta}$.

Stress Evolution and Thermal Effects

In the stress evolution equation,

$$\overset{\nabla}{\mathbf{T}} = \mathbb{L}\left[\mathbf{D} - \mathbf{D}^p\right] - \mathbf{\Pi}\dot{\theta},$$

the term $\mathbf{\Pi}\dot{\theta}$ represents the stress change that would occur due to pure thermal expansion alone, without any mechanical loading.

Summary:

- Thermal expansion induces str
- Subtracting $\mathbf{\Pi}\dot{\theta}$ ensures only r
- This keeps the constitutive mo

Why Subtract the Thermal Term?

- Thermal expansion creates strain even without external forces.
- Without subtracting $\mathbf{\Pi}\dot{\theta}$, the model would falsely attribute thermal strain as mechanical stress.
- Subtracting isolates the true mechanical response from thermal effects.

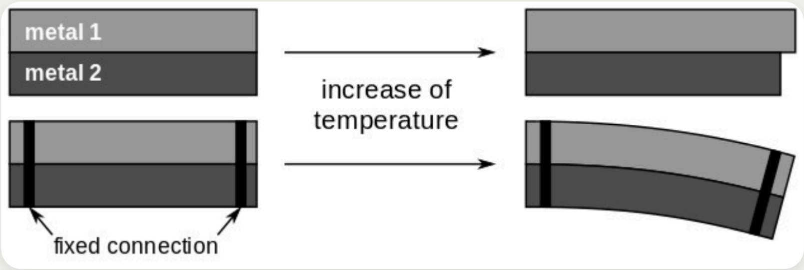

rain without force.
mechanical strains generate stresses.
del physically accurate during heating and cooling.

Context for the Relaxed Configuration

- The relaxed configuration represents the material after removing plastic deformations but before applying new elastic deformations.
- It is introduced to separate permanent plastic effects from recoverable elastic effects.
- All thermodynamic potentials, internal variables, and evolution laws are defined relative to this frame.
- The relaxed state provides a clean, natural reference for measuring elastic strain E^e and computing dissipation.

Summ

- The relaxed configuration isolates elastic responses c plastic evolution laws.

iate) Configuration

What Happens in the Relaxed Configuration?

- The elastic deformation gradient F^e is measured from the relaxed state to the current deformed state.
- Elastic strain measures like C^e and E^e are defined in this configuration.
- The Kirchhoff stress $\widetilde{\mathbf{T}}$ is naturally associated with the relaxed volume.
- Plastic flow is accounted for separately through the plastic velocity gradient $\mathbf{L}^p$.

---

mary:

cleanly, enabling proper definition of thermodynamics and

Kinematics in the Relaxed Configuration

- Elastic deformation gradient:

$$F = F^e F^p \quad \Rightarrow \quad F^e = F F^{p-1}$$

- Elastic right Cauchy-Green tensor:

$$C^e = F^{eT} F^e$$

- Elastic Green–Lagrange strain tensor:

$$E^e = \frac{1}{2}(C^e - I)$$

Sumı

- Elastic kinematics and stress measures are formulate plastic and elastic contributions.
- Stress Power Split allows Anand to cleanly isolate pla
- Green-Lagrange strain tensor E^e is used because it s relaxed configuration
- The right Cauchy-Green tensor $C^e = F^{e^T} F^e$ is requi deformation gradient F^e without referencing spatial c

Stress and Power Quantities

- Kirchhoff stress (weighted Cauchy stress):

$$\widetilde{\mathbf{T}} = (\det F)\mathbf{T}$$

- Stress power split:

$$\dot{\omega} = \dot{\omega}^e + \dot{\omega}^p$$

$$\dot{\omega}^e = \widetilde{\mathbf{T}} : \dot{E}^e \quad , \quad \dot{\omega}^p = (C^e \widetilde{\mathbf{T}}) : \mathbf{L}^p$$

---

mary:

ed relative to the relaxed configuration, cleanly separating

astic dissipation from elastic storage.

symmetrically captures nonlinear elastic strain relative to the

red as an intermediate to compute E^e from the elastic

coordinates

Thermodynamic Separation

1. **Start with Total Dissipation:**

$$\mathcal{D} = \dot{\omega} - \dot{\psi} \geq 0$$

where $\dot{\omega} = \widehat{\mathbf{T}} : \dot{\mathbf{E}}^e + (\mathbf{C}^e \widehat{\mathbf{T}}) : \mathbf{L}^p$

2. **Split Stress Power:**

$$\dot{\omega} = \dot{\omega}^e + \dot{\omega}^p$$

with:

- $\dot{\omega}^e = \widehat{\mathbf{T}} : \dot{\mathbf{E}}^e$
- $\dot{\omega}^p = (\mathbf{C}^e \widehat{\mathbf{T}}) : \mathbf{L}^p$

3. **Group Terms with $\dot{\psi}$:**

$$(\dot{\omega}^e - \dot{\psi}) + \dot{\omega}^p \geq 0$$

4. **Apply Elastic Energy Consistency:**

$$\dot{\omega}^e - \dot{\psi} = 0 \quad \Rightarrow \quad \dot{\omega}^p \geq 0$$

Key Physical Insights

- **Elastic deformations** are recoverable and do not cause entropy production.
- **All dissipation** stems from the plastic flow: $\dot{\omega}^p$.
- **Plastic work** increases entropy and governs viscoplastic evolution.

Summary:
The stress power split ensures that the second law is satisfied by assigning dissipation solely to irreversible processes.

Framework in the Reference Configuration

- The free energy ψ is defined relative to the reference configuration.
- State variables like $E^e, \theta, \bar{g}, \bar{\mathbf{B}}, s$ are used as arguments of ψ.
- Stress is expressed using the second Piola–Kirchhoff tensor $\mathbf{S}$.
- Dissipation inequality, stress–strain relations, and evolution laws are all written in reference variables.
- Mass density ρ_0 from the reference configuration normalizes all terms.

Summ

- In the reference configuration, all energy storage, stre
with reference-frame quantities for consistency and o

Key Equations in the Reference Frame

- Free energy:

$$\boxed{\psi = \psi(E^e, \theta, \bar{g}, \bar{\mathbf{B}}, s)}$$

- Dissipation inequality:

$$\boxed{\dot{\psi} + \eta\dot{\theta} - \rho_0^{-1}\mathbf{S} : \dot{E} + (\rho_0\theta)^{-1}\mathbf{q}_0 \cdot \mathbf{g}_0 \leq 0}$$

- Constitutive relation:

$$\boxed{\mathbf{S} = \rho_0 \frac{\partial \psi}{\partial E^e}}$$

mary:

ess updates, and internal variable evolution are formulated
bjectivity.

Thermodynamic Quantities

- Free energy density:

$$\boxed{\psi = \epsilon - \theta\eta}$$

- Reduced dissipation inequality:

$$\boxed{\dot{\psi} + \eta\dot{\theta} - \rho^{-1}\mathbf{T} : \mathbf{L} + (\rho\theta)^{-1}\mathbf{q} \cdot \mathbf{g} \leq 0}$$

- State variables:

$$\{E^e, \theta, \bar{g}, \bar{\mathbf{B}}, s\}$$

with E^e as elastic strain and s as internal resistance.

Summary:
- Free energy and dissipation
- Stress power naturally split
- Kirchhoff stress simplifies s

Stress Power and Kirchhoff Stress

- Stress power per relaxed volume:

$$\boxed{\dot{\omega} = \left(\frac{\rho_0}{\rho}\right) \mathbf{T} : \mathbf{L}}$$

- Weighted Cauchy (Kirchhoff) stress:

$$\boxed{\widetilde{\mathbf{T}} = (\det F)\mathbf{T}} \quad \text{or} \quad \boxed{\widetilde{\mathbf{T}} = \left(\frac{\rho_0}{\rho}\right) \mathbf{T}}$$

- Decomposition of stress power:

$$\boxed{\dot{\omega} = \dot{\omega}^e + \dot{\omega}^p}$$

$$\dot{\omega}^e = \widetilde{\mathbf{T}} : \dot{E}^e, \quad \dot{\omega}^p = (C^e \widetilde{\mathbf{T}}) : \mathbf{L}^p$$

n govern thermodynamic consistency.
s into elastic and plastic parts.
stress evolution accounting for volume changes.

Multichamber

Michael Raba, MSc Candida

Created: 2025-0

Muffler System

ate at University of Kentucky

5-28 Wed 04:40

der Internal Geometry

Dimen

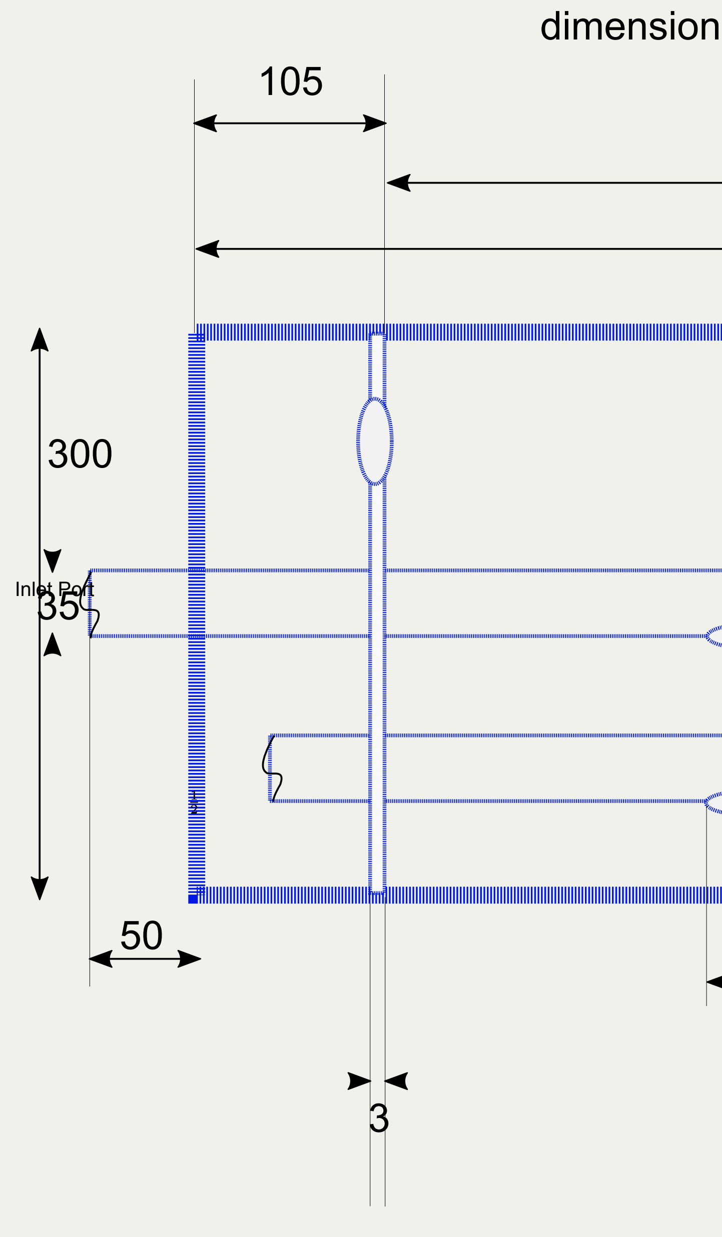

nsions

al units in mm

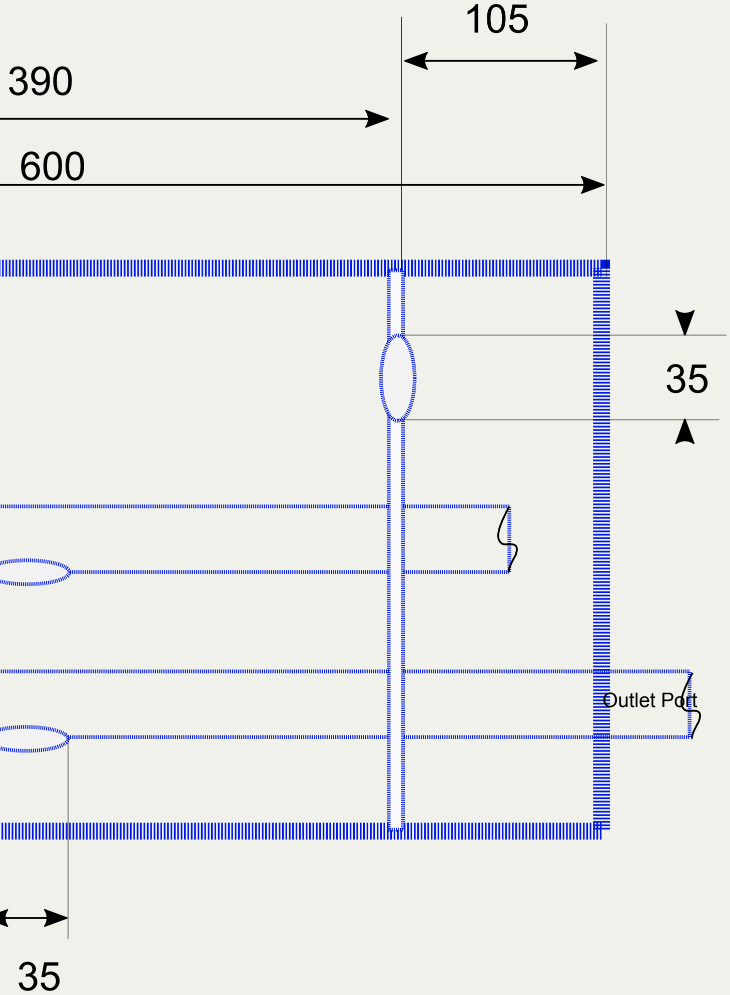

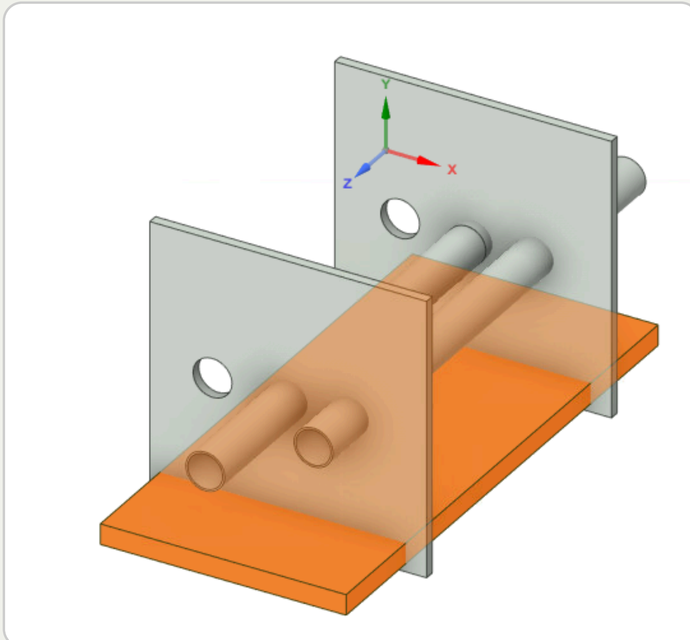

Part 1 — Chamber and Baffle

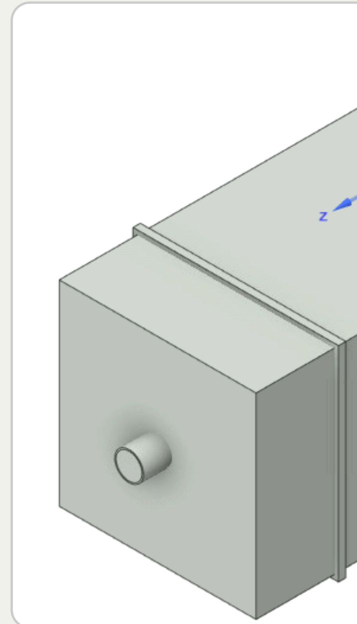

Part 2 — Fl

Part 4 — Showing perforates (aimed at fiberglass)

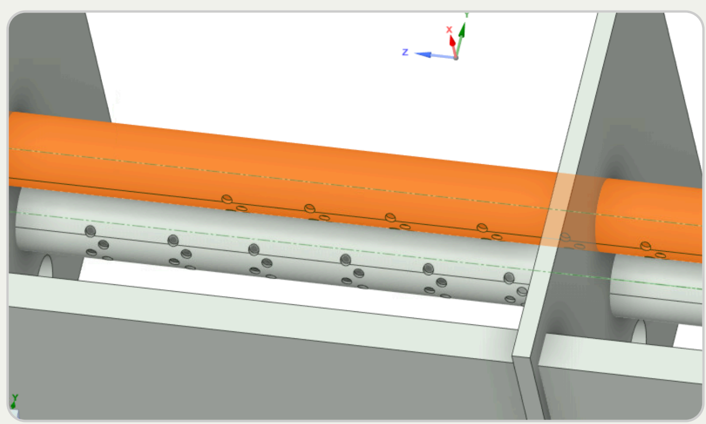

Muffler Subcomponents

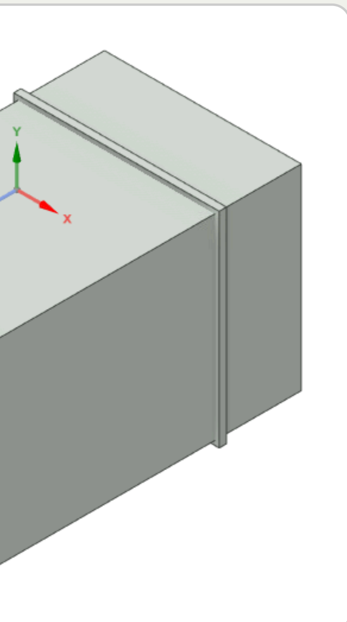

luid domain

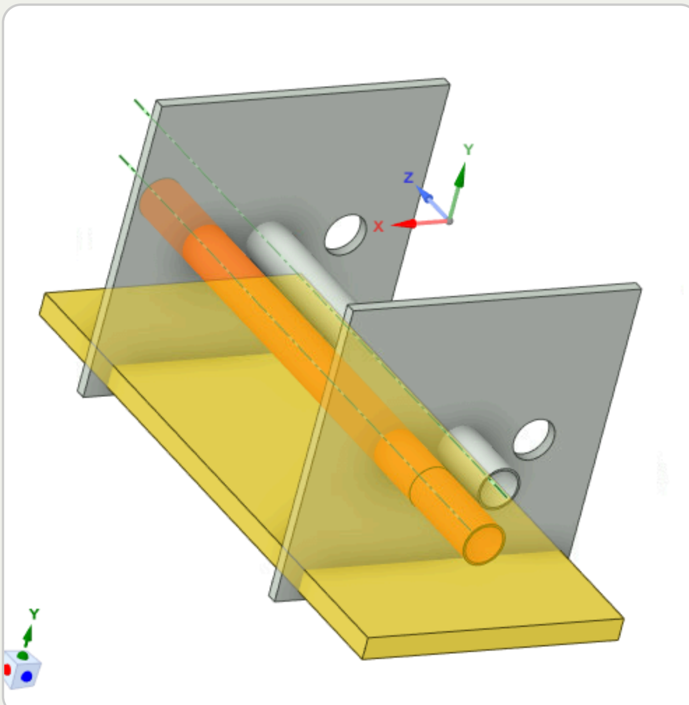

Part 3 — Fiberglass Absorbant (gold)

Part 5 — Final Assembly View

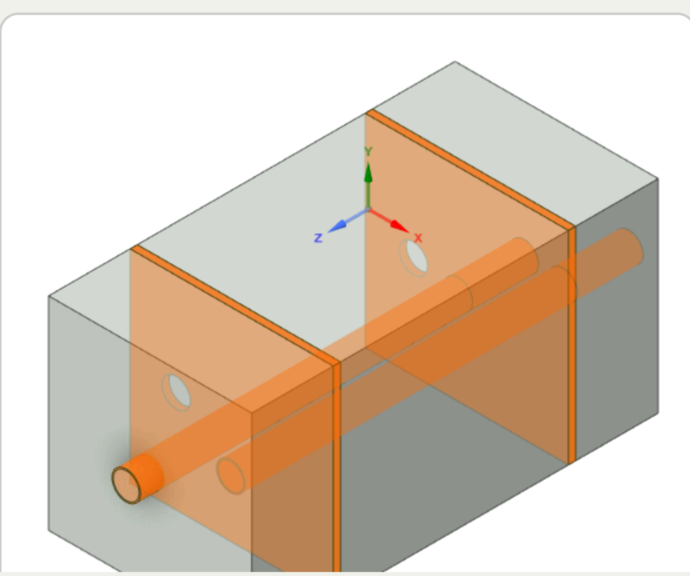

Ansys Si

Simulated Transmission Loss (0–1000 Hz) by a

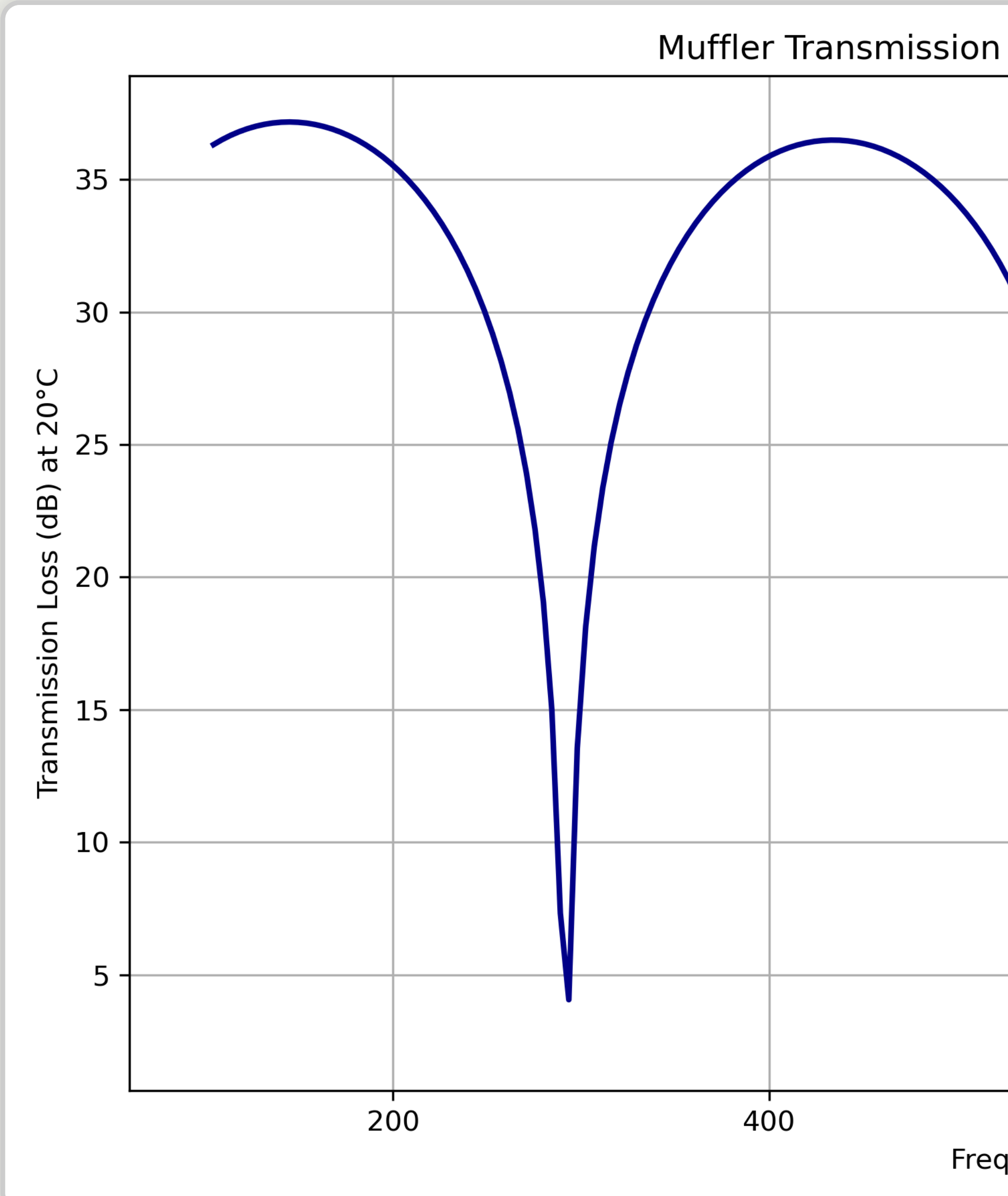

Figure: Transmission Loss curve of the m mulation

approximating muffler walls as fluid at 20 deg C

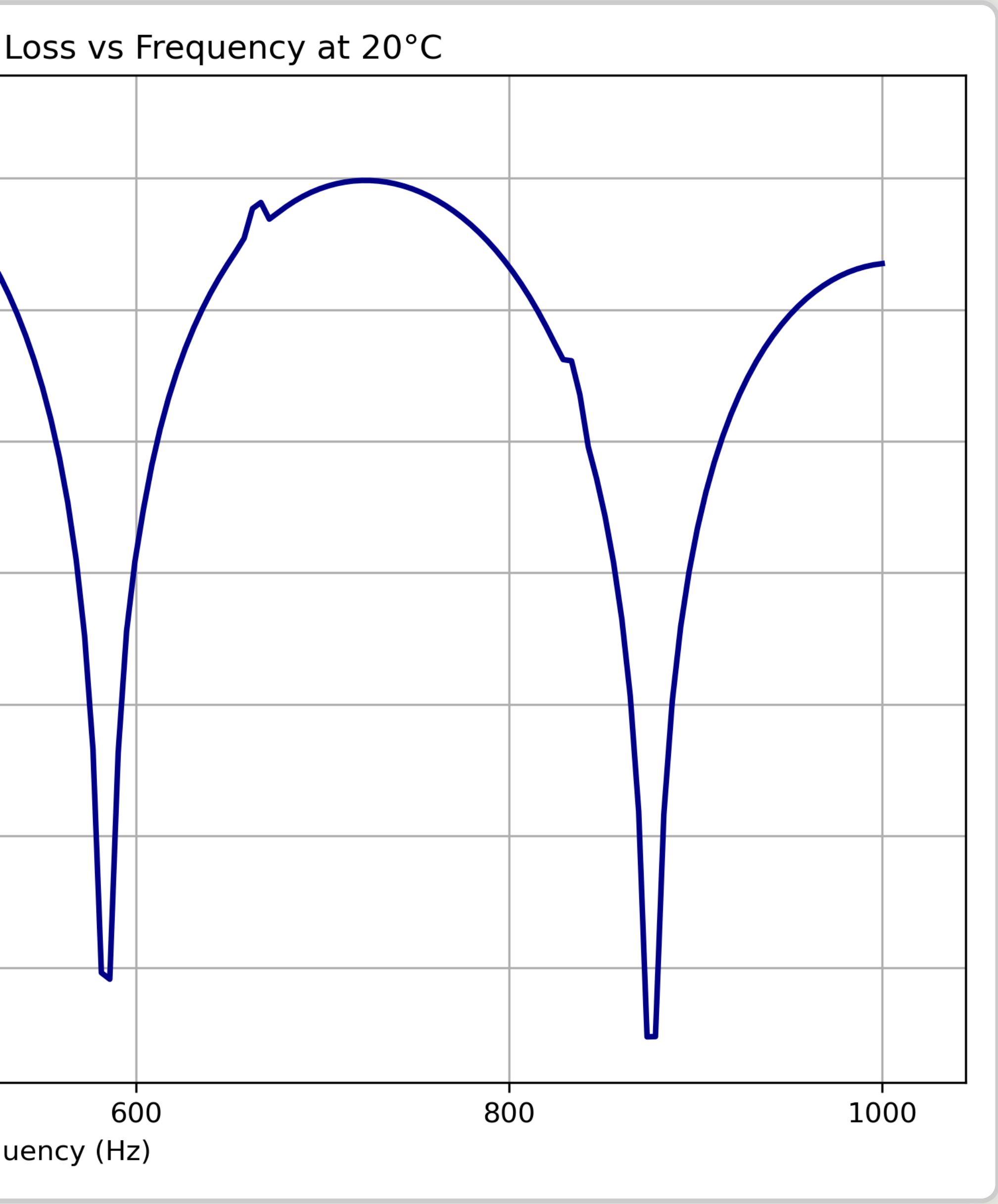

uffler between 5 Hz and 1000 Hz at 20°C.

Simulated Transmission Loss

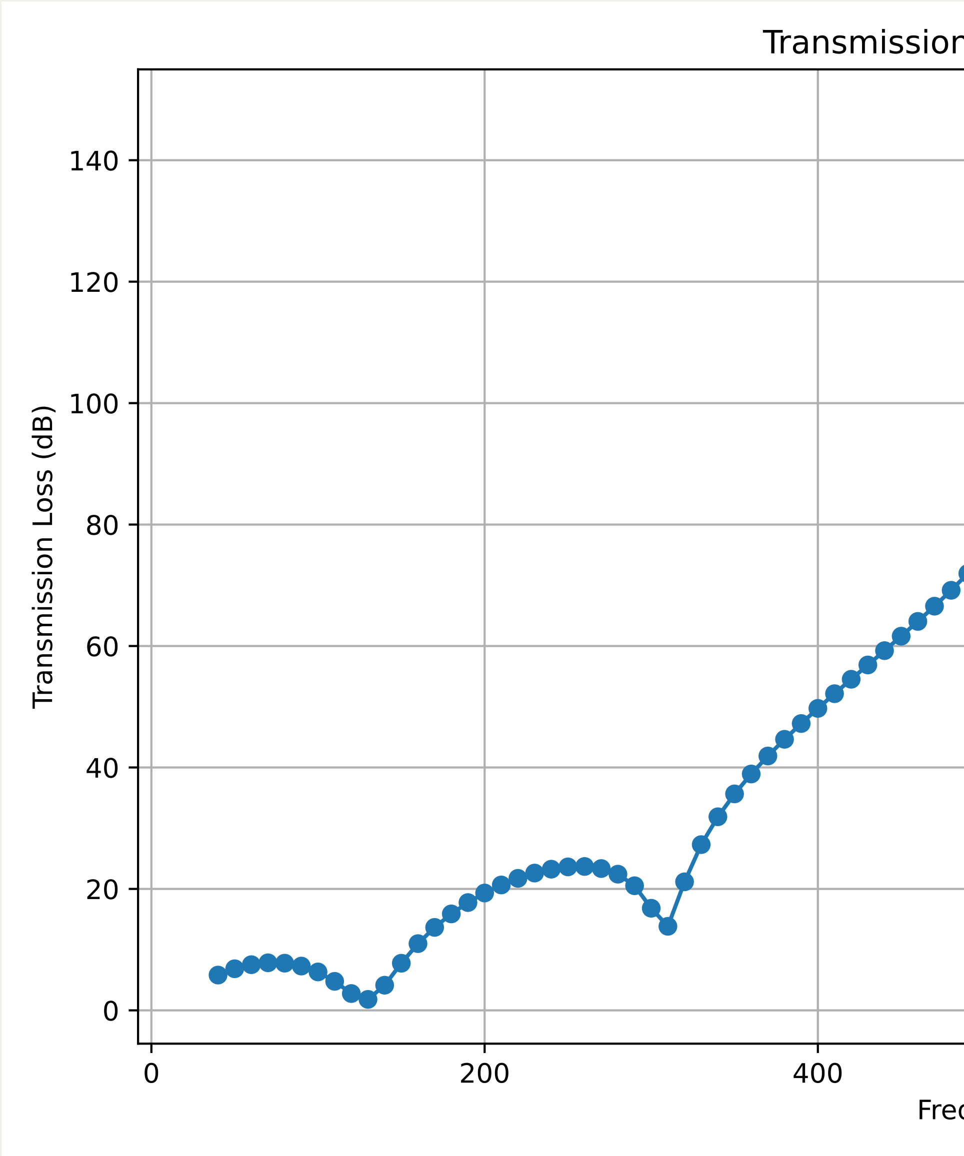

imulation

s (0–1000 Hz) Simlab model

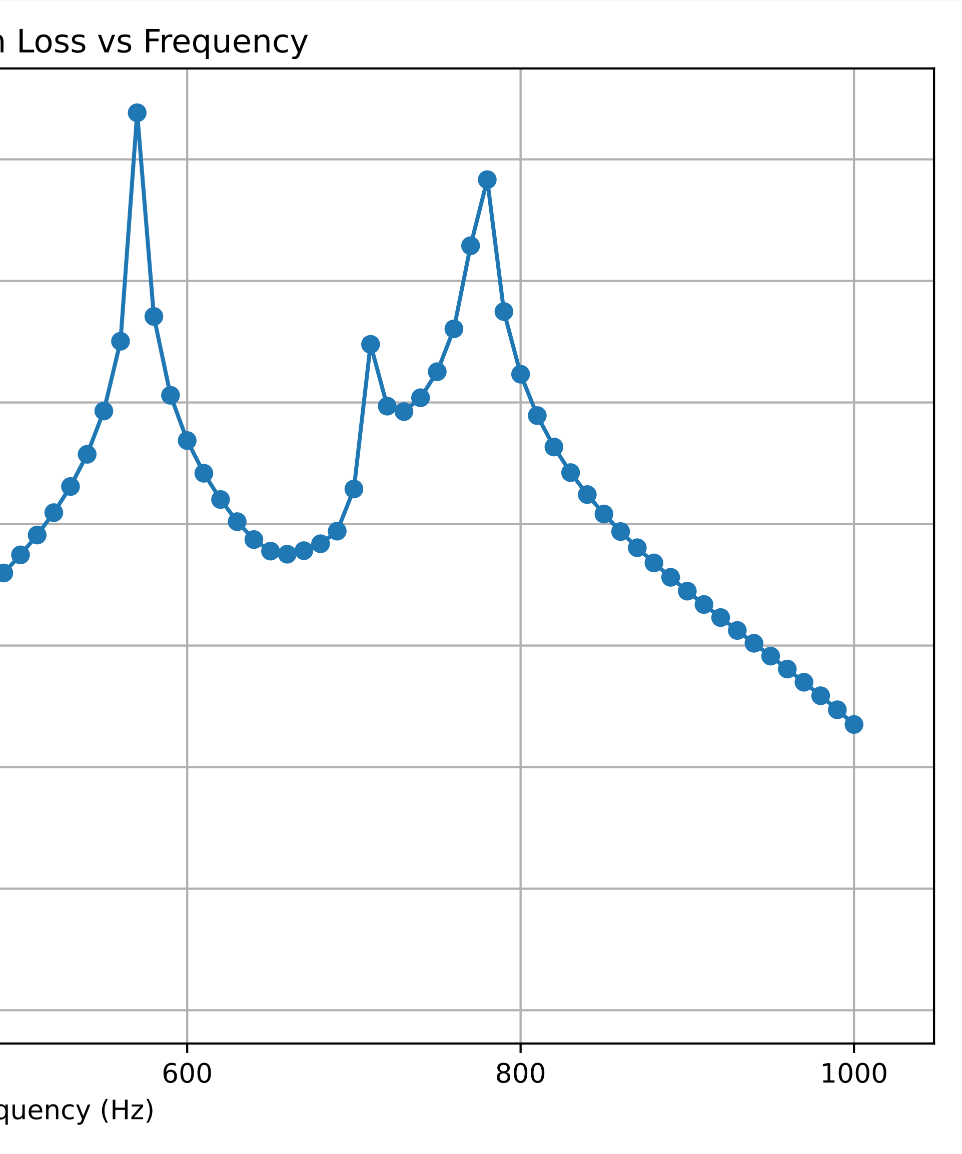

Sidlab and Ansys Fi

SIDLAB Model

- **File:** `Mark3Sid.zip`
- **Created with:** SIDLAB 5.1
- ⬇ **Download SIDLAB File**

le Download Center

ANSYS Simulation

- **File:** `Mark-I-MDF-clearned-data.wbpz`
- **Created with:** ANSYS 2023 R2
- **⬇ Download ANSYS File**

dimension

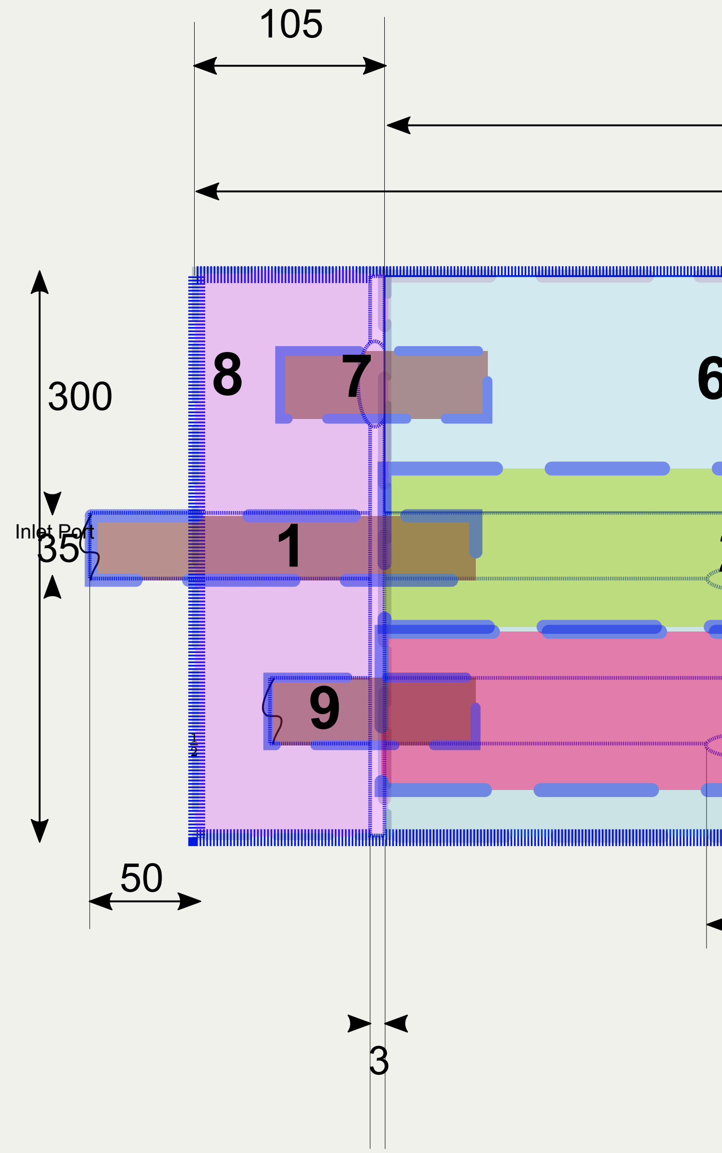

mponents

al units in mm

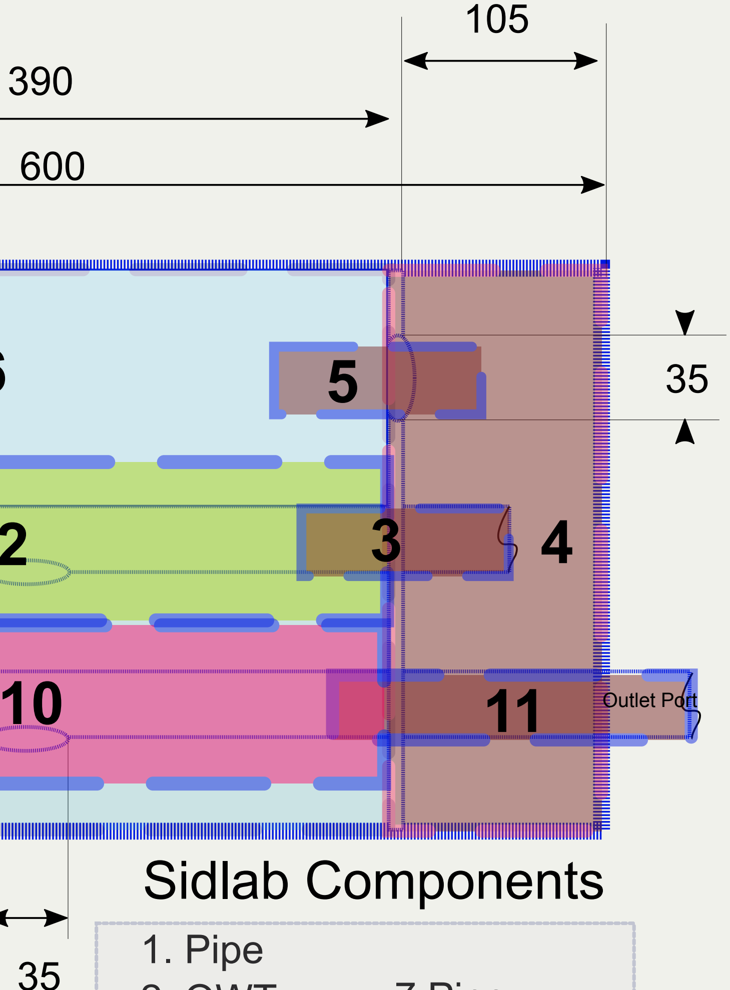

Sidlab Components

1. Pipe
2. QWT
3. Pipe
4. QWT
5. Pipe
6. QWT
7. Pipe
8. QWT
9. Pipe
10. QWT
11. Pipe

Simulated vs Meas

Measured vs Simulated TL

ured Insertion Loss

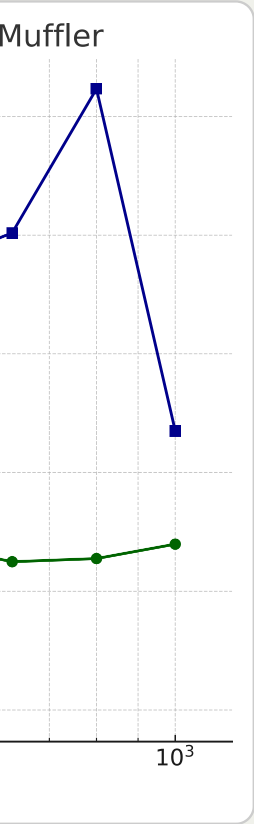

Insertion Loss Explanation

Insertion Loss (IL) quantifies how much sound is attenuated when a muffler is added to the system.

General formula:

$$\mathrm{IL} = 10\log_{10}\left(\frac{P_{\text{baseline}}}{P_{\text{muffler}}}\right)$$

Because our data is already in decibels (dB), this simplifies to:

$$\mathrm{IL} = \mathrm{Power}_{\text{baseline (dB)}} - \mathrm{Power}_{\text{muffler (dB)}}$$

Refer

Cited

1. Munjal ML. *Acoustics of Ducts and Mufflers*. 2nd ed. W
   https://doi.org/10.1002/9781118443125
2. Dokumacı E. *Duct Acoustics: Fundamentals and Appli*
   Press; 2021. ISBN: 9781108840750. https://doi.org/10

Note: These references are foundational texts in muffler ar
schematic development, an

ences

Works

Wiley; 2014. ISBN: 9781118443125.

cations to Mufflers and Silencers. Cambridge University

.1017/9781108840750

---

nd duct acoustics and were consulted for system modeling,
d transmission loss analysis.

POD Analysis of T

M. F

Created: 2025-0

urbulent Pipe Flow

Raba

9-10 Wed 03:38

1. Code Execut

tion and Layout

1. b7.m
2. initSpectral.m
    - reads i
3. ↪ initEigs.m
    - forms

ayout

in binary files, takes eg m-fft

corrMat, finds eigenvalues

1. ↪ initPod.m
    - carries out POD calculations (quadrature, multiplication
      Hellstrom Smits 2017 for Snapshot POD)
2. ↪ timeReconstructFlow.m
    - performs 2d reconstruction + plotSkmr (generates 1d ra

ayout 2

ggf betwen $\alpha\Phi$) according to Papers (Citriniti George 2000 for Classic POD,

dial graph)

pipe = Pipe(); creates a Pipe Class. As the functio

1. obj.CaseId - stores properties like Re, rotation number S, experiment
   frequently called vectors (rMat $r = 1, \ldots, 0.5$)
2. obj.pod - eigen data, used for calculating POD
3. obj.solution - computed POD modes
4. obj.plt - plot configuration

ant Switches

ns (above) are called, data is stored in sub-structs:

tal flags such as quadrature (simpson/trapezoidal), number of gridpoints,

2. Equations Used

in Code Procedure

The following equations a

$$\int_{r'} \mathbf{S}\left(k;m;r,r'\right)\Phi^{(n)}\left(k;m;r'\right)$$

$$\mathbf{S}\left(k;m;r,r'\right) = \lim_{\tau\to\infty}\frac{1}{\tau}\int_0^{\tau}\mathbf{u}(k$$

$$\alpha^{(n)}(k;m;t) = \int_r \mathbf{u}(k;m;r,t)\Phi$$

OD Equations

re used in the above code.

$$r' \mathrm{d}r' = \lambda^{(n)}(k;m)\Phi^{(n)}(k;m;r)$$

$$;m;r,t)\mathbf{u}^{*}\left(k;m;r',t\right)\mathrm{d}t$$

$$^{(n)^{*}}(k;m;r)r\;\mathrm{d}r$$

2.2. Classic POD

$$\int_{r'} \underbrace{r^{1/2} S_{i,j}\left(r, r'; m; f\right) r'^{1}}_{W_{i,j}(r,r';m;f)}$$

$$= \underbrace{\lambda^{(n)}(m, f)}_{\hat{\lambda}^{(n)}(m;f)} \underbrace{r^{1/2} \phi_i^{(n)}(r;}_{\hat{\phi}_i^{(n)}(r,m;}$$

$$\alpha_n(m;t) = \int_r \mathbf{u}(m;r,t)r$$

Equations (Fixed)

$$\ldots^{1/2}\underbrace{\phi_j^{*(n)}\left(r';m;f\right)r'^{1/2}}_{\hat{\phi}_j^{\psi(i)}(r';m;f)}\mathrm{d}r'$$

$$\underbrace{\ldots m;f)}_{\ldots f)}$$

$$\ldots^{1/2}\Phi_n^*(m;r)dr$$

$$\lim_{\tau\to\infty}\frac{1}{\tau}\int_0^\tau \mathbf{u}_\mathrm{T}(k;m;r,t)$$

$$= \Phi_\mathrm{T}^{(n)}(k;m;r)\lambda^{(n)}(k;m$$

$$\mathbf{R}\,(k;m;t,t') = \int_r \mathbf{u}(k;r$$

$$\lim_{\tau\to\infty}\frac{1}{\tau}\int_0^\tau \mathbf{u}_\mathbf{T}(k;m;r,t$$

$$= \Phi_\mathbf{T}^{(n)}(k;m;r)\lambda^{(n)}(k;m$$

POD Equations

$$)\alpha^{(n)^*}(k;m;t)\mathrm{d}t$$

$$n)$$

$$n;r,t)\mathbf{u}^*\,(k;m;r,t')\,r\,\mathrm{d}r$$

$$)\alpha^{(n)*}(k;m;t)\,\mathrm{d}t$$

$$n).$$

The reconstruc

$$q(\xi, t) - \bar{q}(\xi) \approx \sum_{j=1}^{r} a_j(t)\varphi_j(\xi)$$

$$q(r, \theta, t; x) = \bar{q}(r, \theta, t; x) +$$

Since the snapshot pod implementation is not error-free, the re

$$q(r, \theta, t; x) = \bar{q}(r, \theta, t; x) + (\text{facto}$$

nstruction

tion is given by

$\Rightarrow$

$$\sum_{n=1} \sum_{m=0} \alpha^{(n)}(m;t)\Phi^{(n)}(r;m;x)$$

construction can only be recovered by writing for factor $\gg 0$.

$$; \gamma) \sum_{n=1} \sum_{m=0} \alpha^{(n)}(m;t)\Phi^{(n)}(r;m;x)$$

In order to reconstruct in code, caseId.fluctuation = 'off'. Th

nstruction

his is incorrect. The necessary use of (factor γ) is incorrect

3. Der

To derive the questioned equ

$$\frac{1}{\tau}\int_0^{\tau} \mathbf{u}_{\mathrm{T}}(k;m;r,$$

Substitute $\mathbf{u}_{\mathrm{T}}$ wi

$$\frac{1}{\tau}\int_0^{\tau}\left(\sum_{l}\Phi_{\mathrm{T}}^{(l)}(k;m;r)\alpha^{(l}\right.$$

ivation

uation, consider the integral:

$$t)\alpha^{(n)^*}(k;m;t)dt.$$

ith its expansion:

$$)(k;m;t)\Big)\,\alpha^{(n)^*}(k;m;t)dt.$$

Exchange the order of summation anc

$$\sum_{l} \Phi_{\mathrm{T}}^{(l)}(k;m;r)\left(\frac{1}{\tau}\int_{0}^{\tau} \alpha^{(l}\right.$$

Due to the orthogonality, namely t

$$\langle a^{(n)}\alpha^{(p)}\rangle$$

all terms where $l \neq n$ will vanish, an

$$\Phi_{\mathrm{T}}^{(n)}(k;m;r)\left(\frac{1}{\tau}\int_{0}^{\tau} \alpha^{(n)}\right.$$

This derivation assumes the normalization of modes and their orthogonality,
form that reveals the spatial structure ($\Phi_{\mathrm{T}}^{(n)}$) c

erivation

d integration, and apply orthogonality,

$$ {}^{l)}(k;m;t)\alpha^{(n)^*}(k;m;t)dt\right). $$

hat $\alpha^{(n)}$ and $\alpha^{(p)}$ are uncorrelated

$$ = \lambda^{(n)}\delta_{np} $$

d there remains only the $l = n$ term,

$$ (k;m;t)\alpha^{(n)^*}(k;m;t)dt\right). $$

along with the eigenvalue relationship to simplify the original integral into a
of each mode scaled by its significance $\left(\lambda^{(n)}\right)$.

The cross-correlation tensor $\mathbf{R}$ is defined as $\mathbf{R}\,(k; m; t, t') = \int_r \mathbf{u}(k; m; r,$

$[t \times t']$ tensor. The n POD m

$$\lim_{\tau \to \infty} \frac{1}{\tau} \int_0^{\tau} \mathbf{u}_{\mathrm{T}}(k; m; r, t)\alpha^{(n)^*}(k;$$

erivation

$t)\mathbf{u}^*\left(k;m;r,t'\right) r\ \mathrm{d}r$. This tensor is now transformed from $[3r \times 3r']$ to a
nodes are then constructed as,

$$n;t)\mathrm{d}t = \Phi_{\mathrm{T}}^{(n)}(k;m;r)\lambda^{(n)}(k;m).$$

4. Result Compariso

on Classic/Snapshot

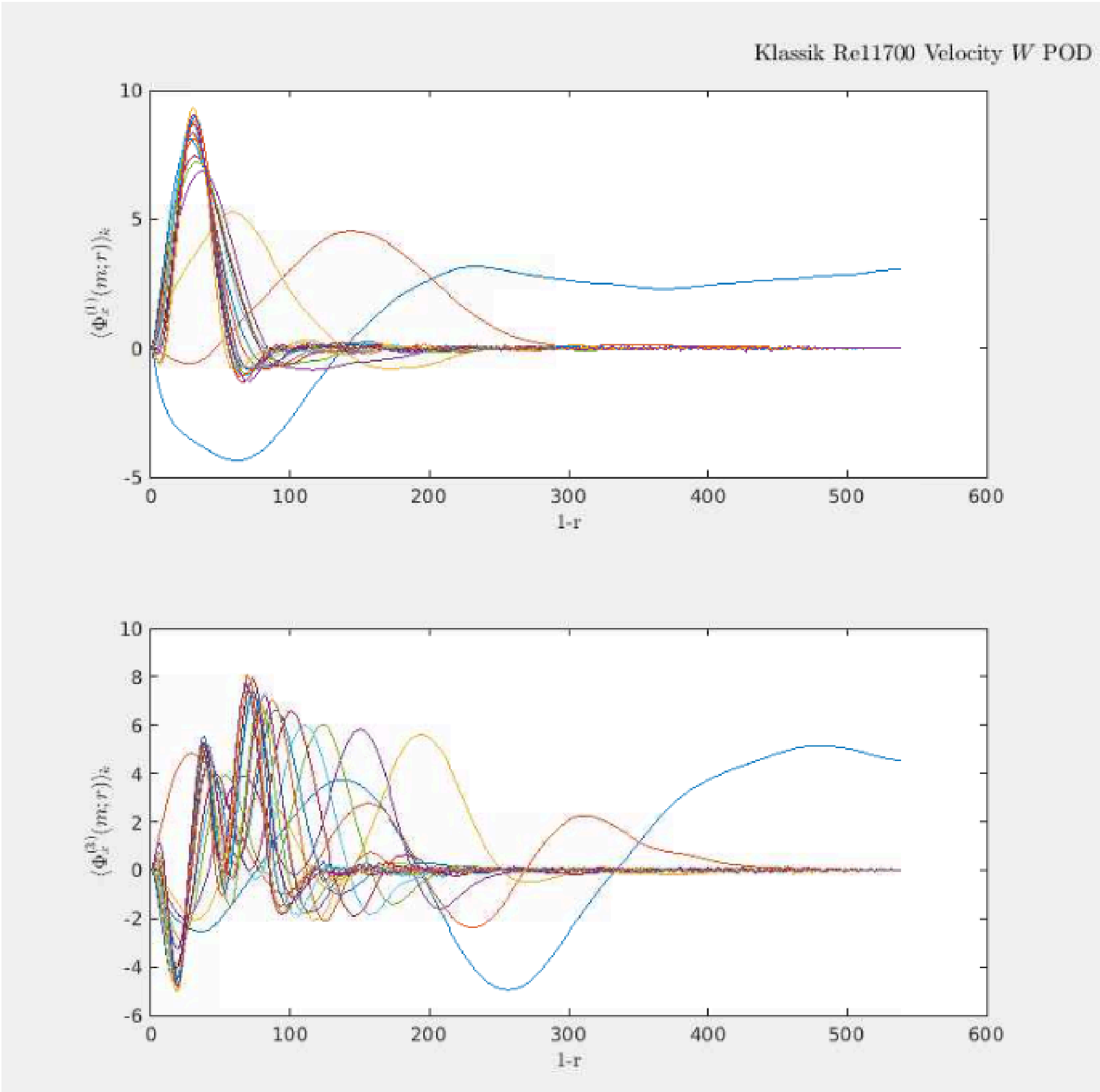
Klassik Re11700 Velocity W POD
$\langle\Phi_z^{(1)}(m;r)\rangle_k$
1-r
$\langle\Phi_z^{(3)}(m;r)\rangle_k$
1-r

al Classic

for Rotation Number $N = 3.0$

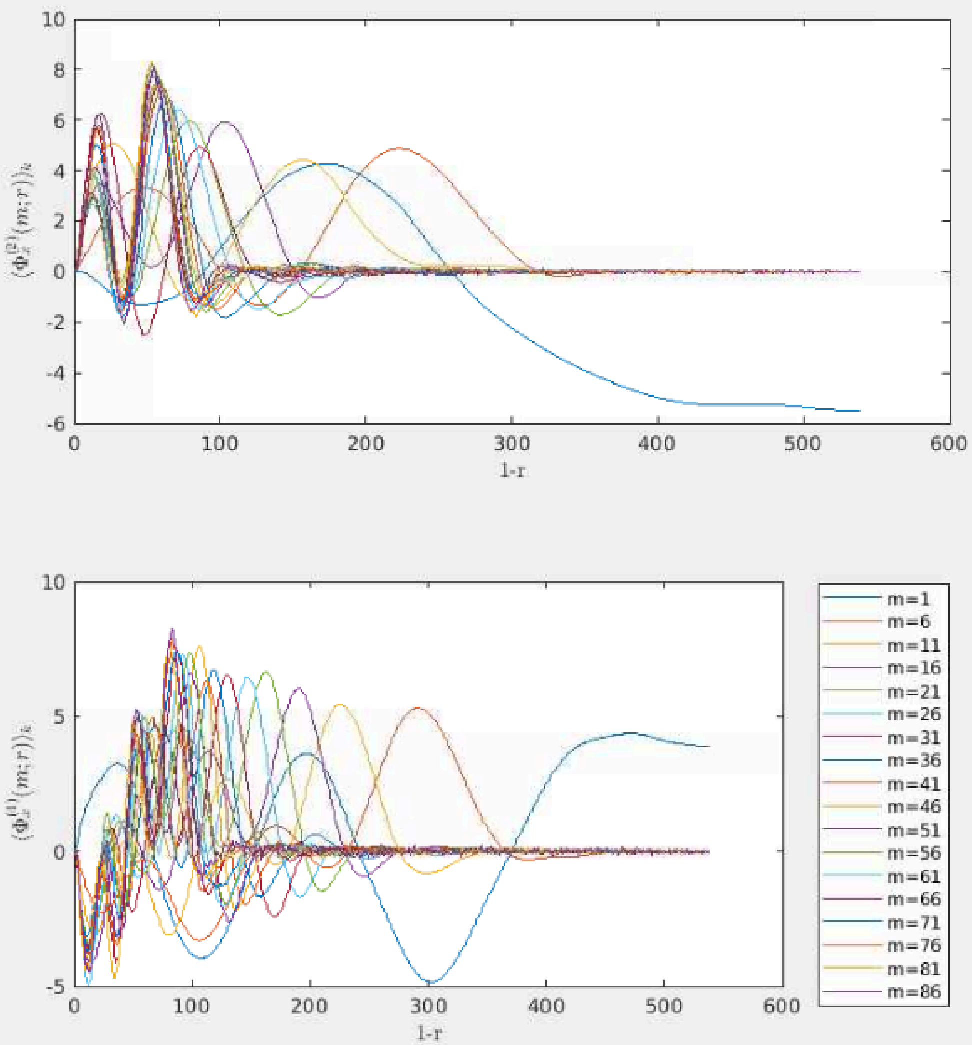

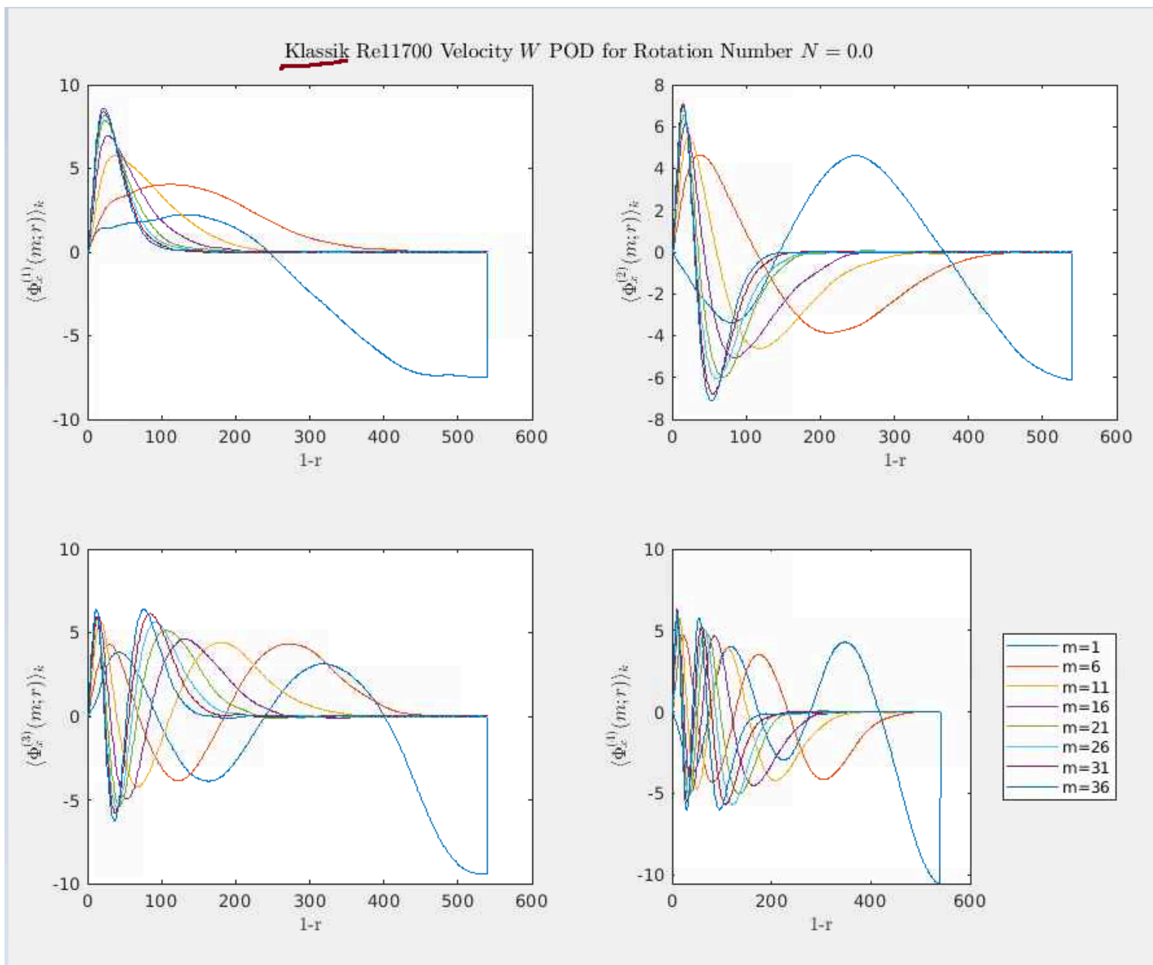
Klassik Re11700 Velocity W POD for Rotation Number $N = 0.0$
$\langle\Phi_x^{(1)}(m;r)\rangle_k$
$\langle\Phi_x^{(2)}(m;r)\rangle_k$
$\langle\Phi_x^{(3)}(m;r)\rangle_k$
$\langle\Phi_x^{(4)}(m;r)\rangle_k$
1-r
m=1
m=6
m=11
m=16
m=21
m=26
m=31
m=36

assic Comparison

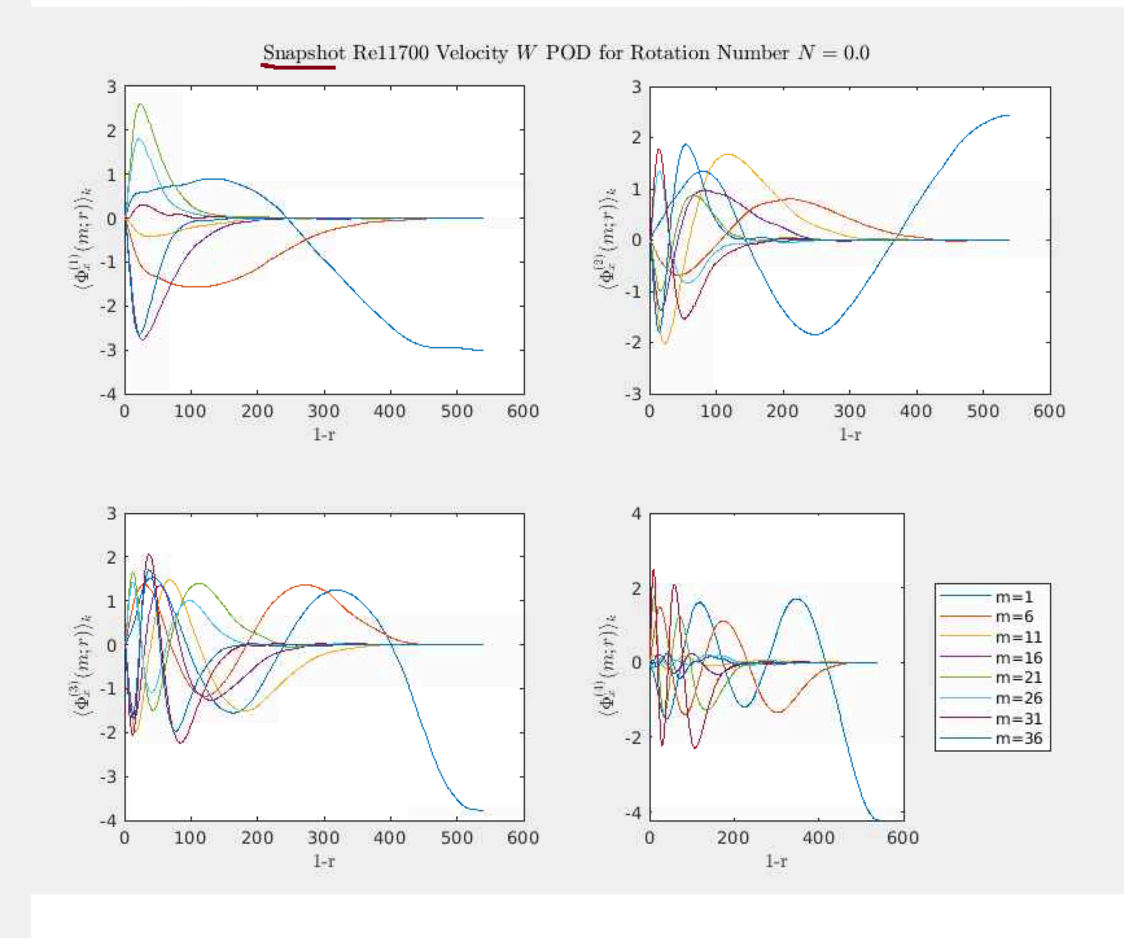

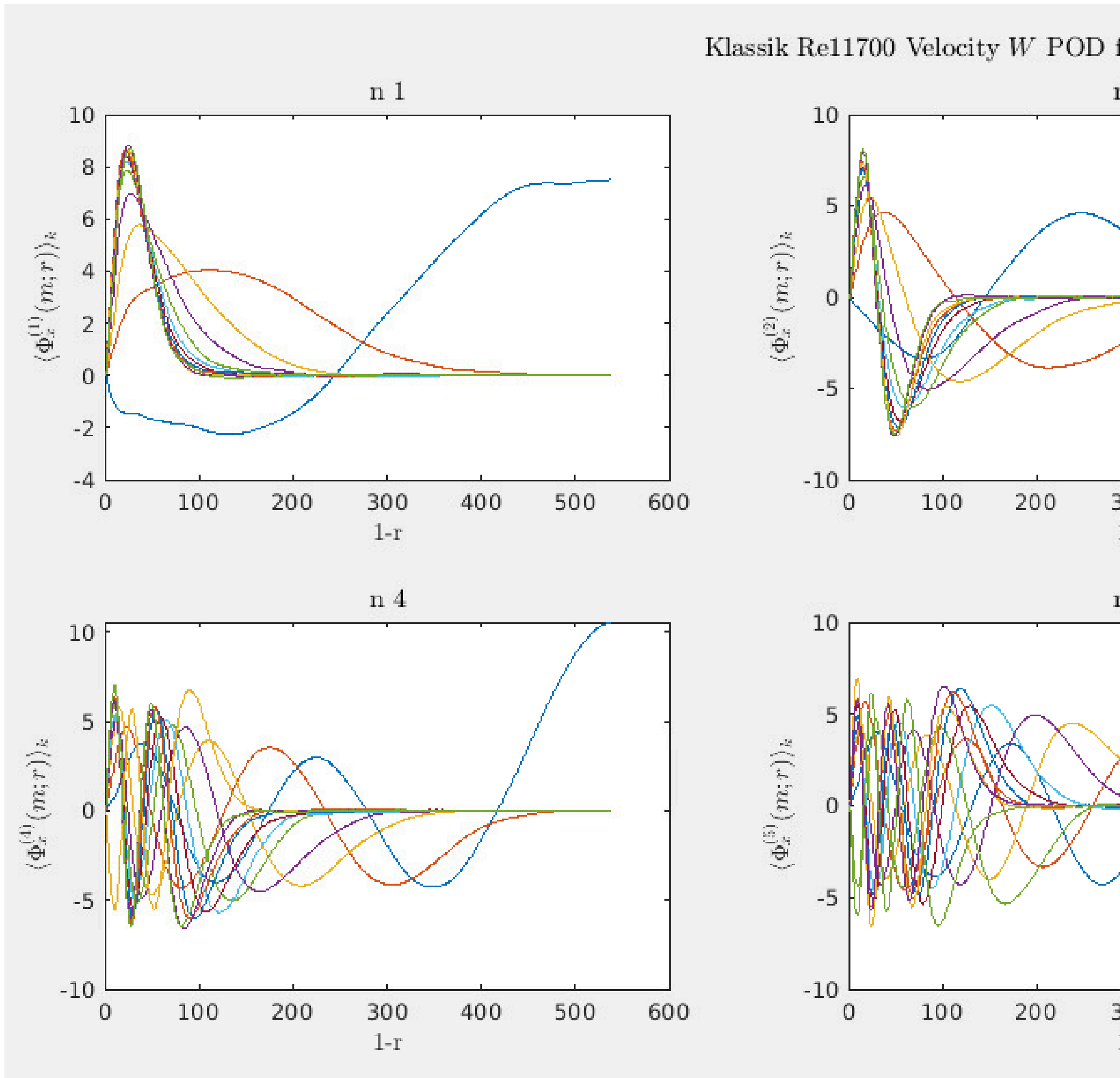
Klassik Re11700 Velocity W POD f
n 1
1-r
n 4
1-r

POD S=0.0

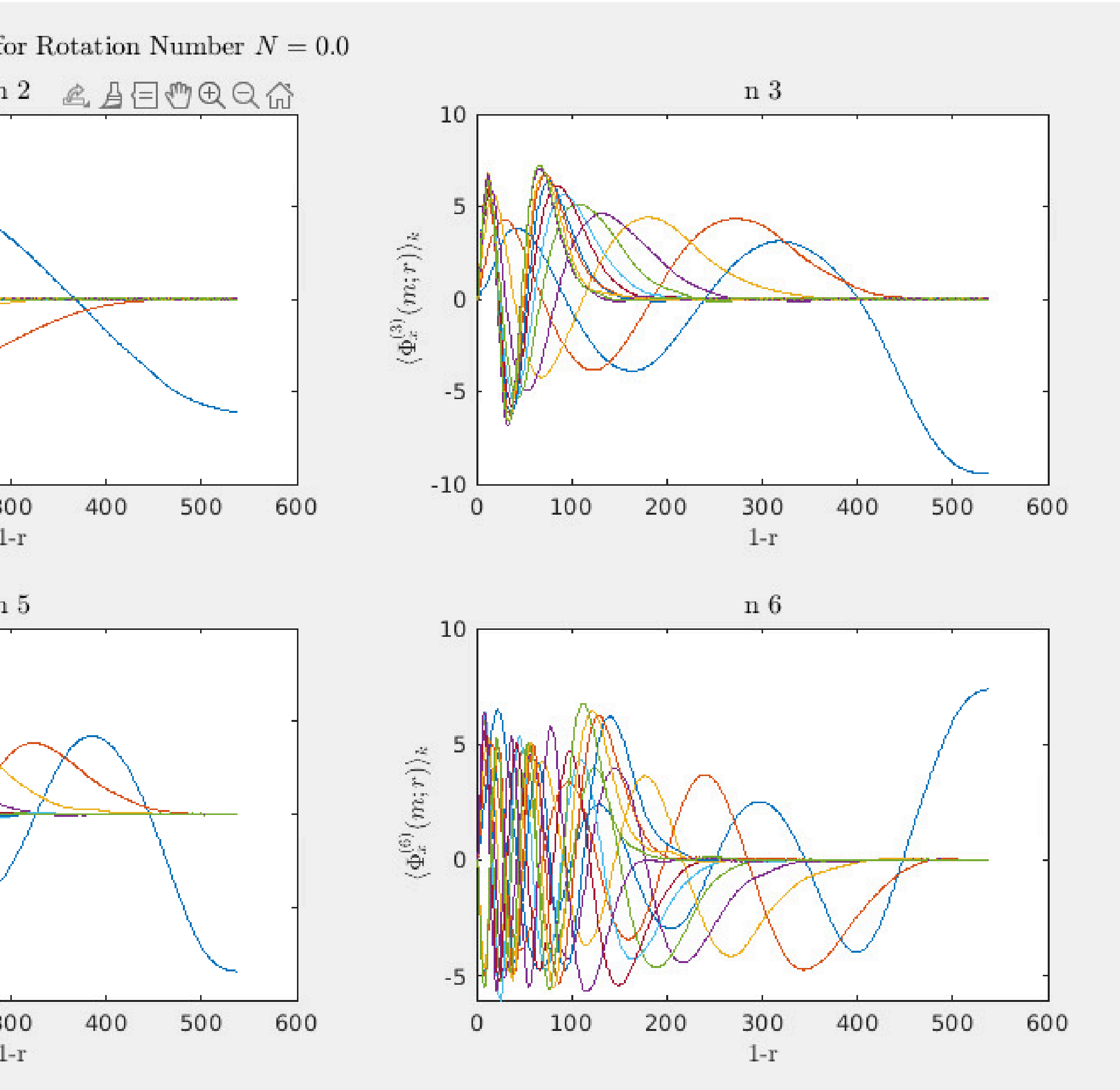
for Rotation Number $N = 0.0$
n 2
n 3
n 5
n 6
1-r
$\langle \Phi_x^{(3)}(m;r) \rangle_k$
$\langle \Phi_x^{(6)}(m;r) \rangle_k$

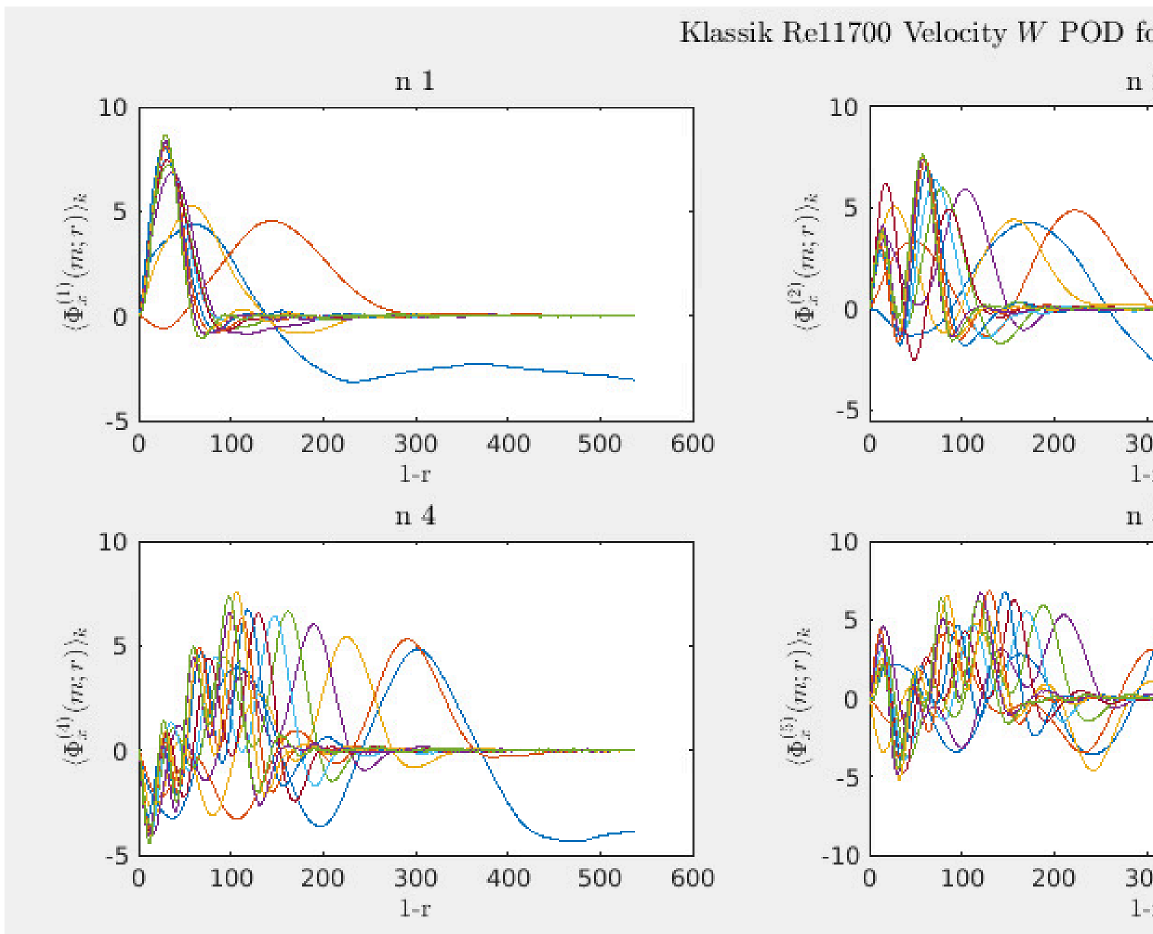
Klassik Re11700 Velocity W POD fo
n 1
n 4
1-r

POD S=3.0

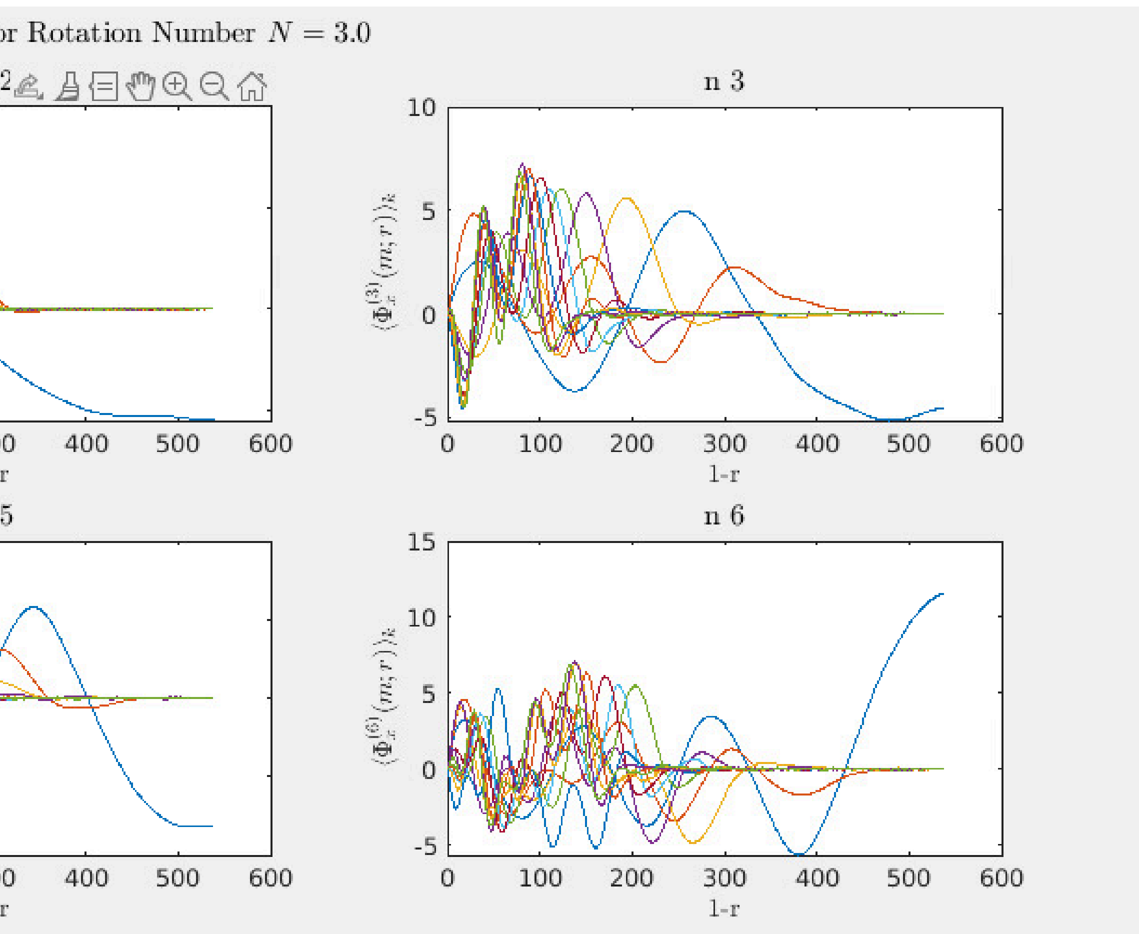
or Rotation Number $N = 3.0$
n 3
n 6
1-r
$\langle \Phi_x^{(3)}(m;r) \rangle_k$
$\langle \Phi_x^{(6)}(m;r) \rangle_k$

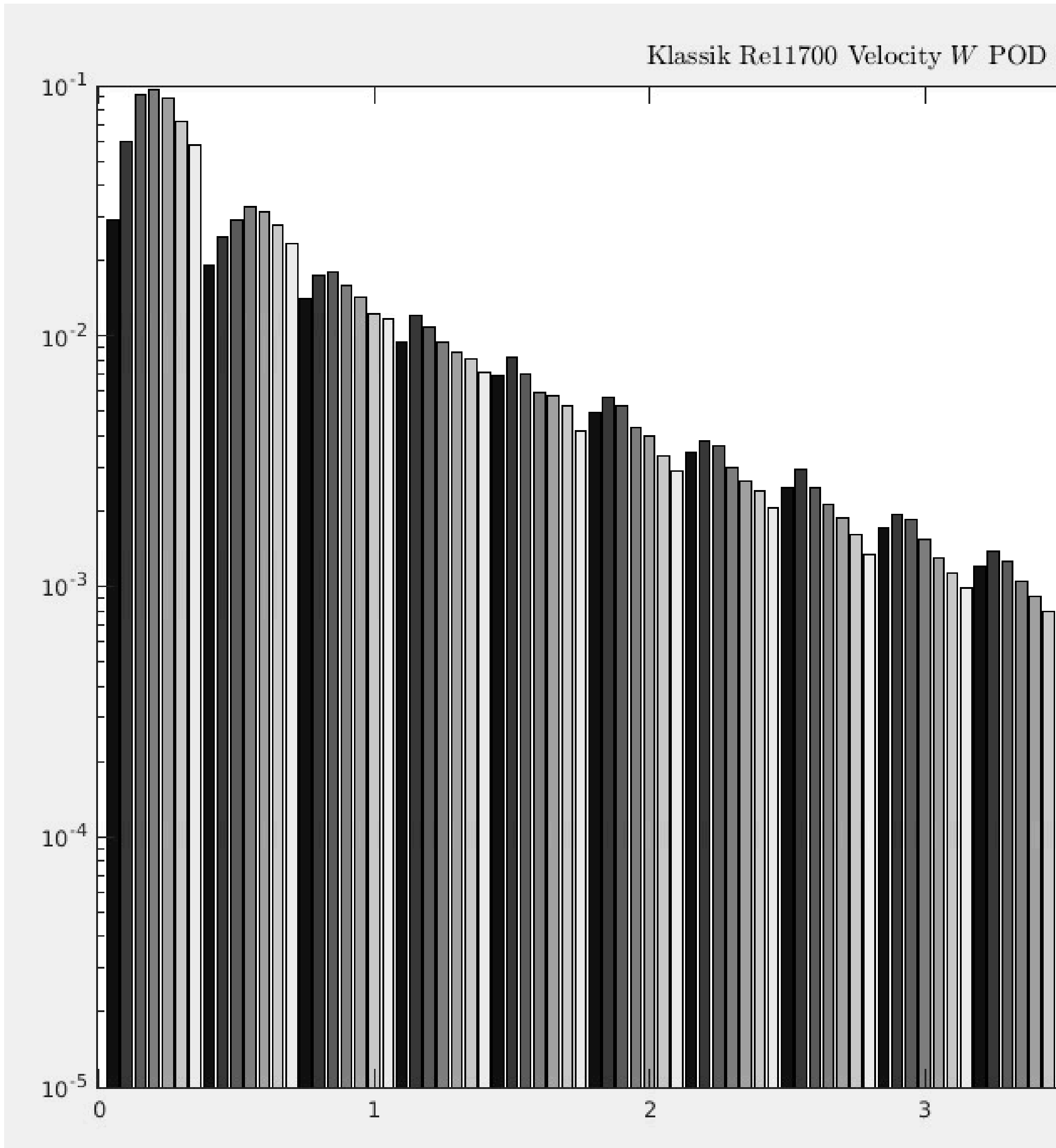
Klassik Re11700 Velocity W POD
10-1
10-2
10-3
10-4
10-5
0
1
2
3

n=0 Classic

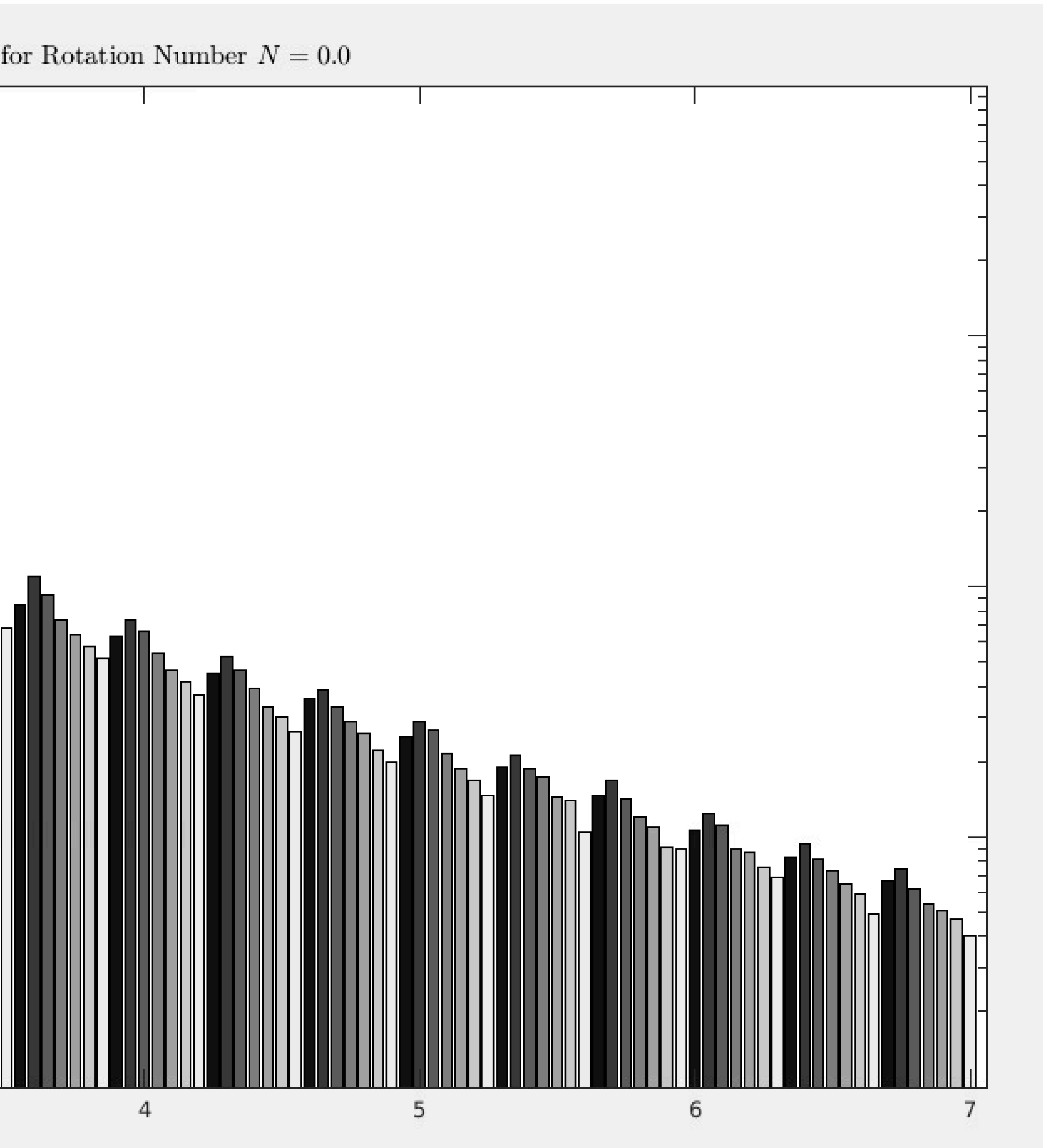

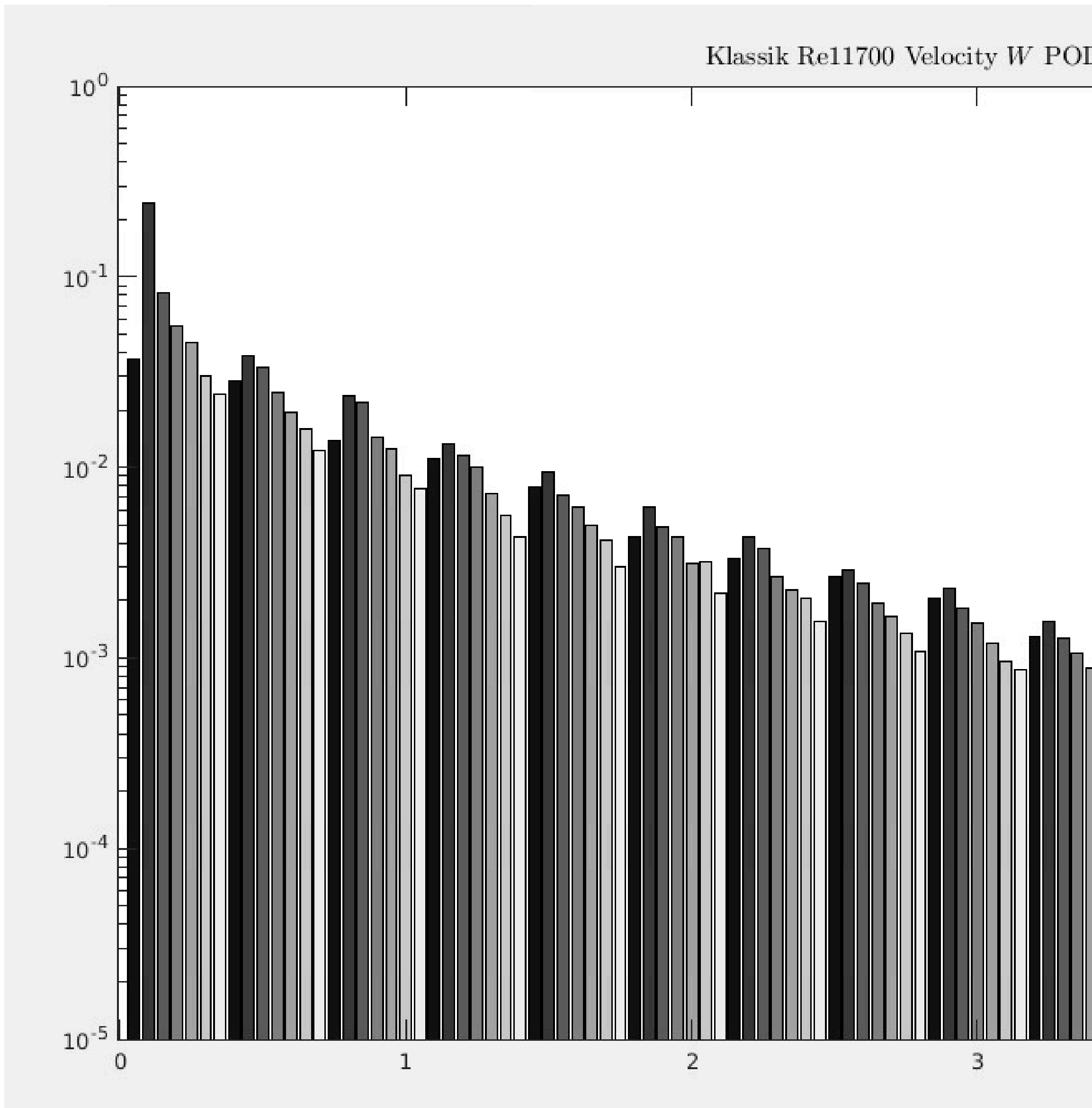
Klassik Re11700 Velocity W POD
10^0
10^-1
10^-2
10^-3
10^-4
10^-5
0
1
2
3

3 Classic

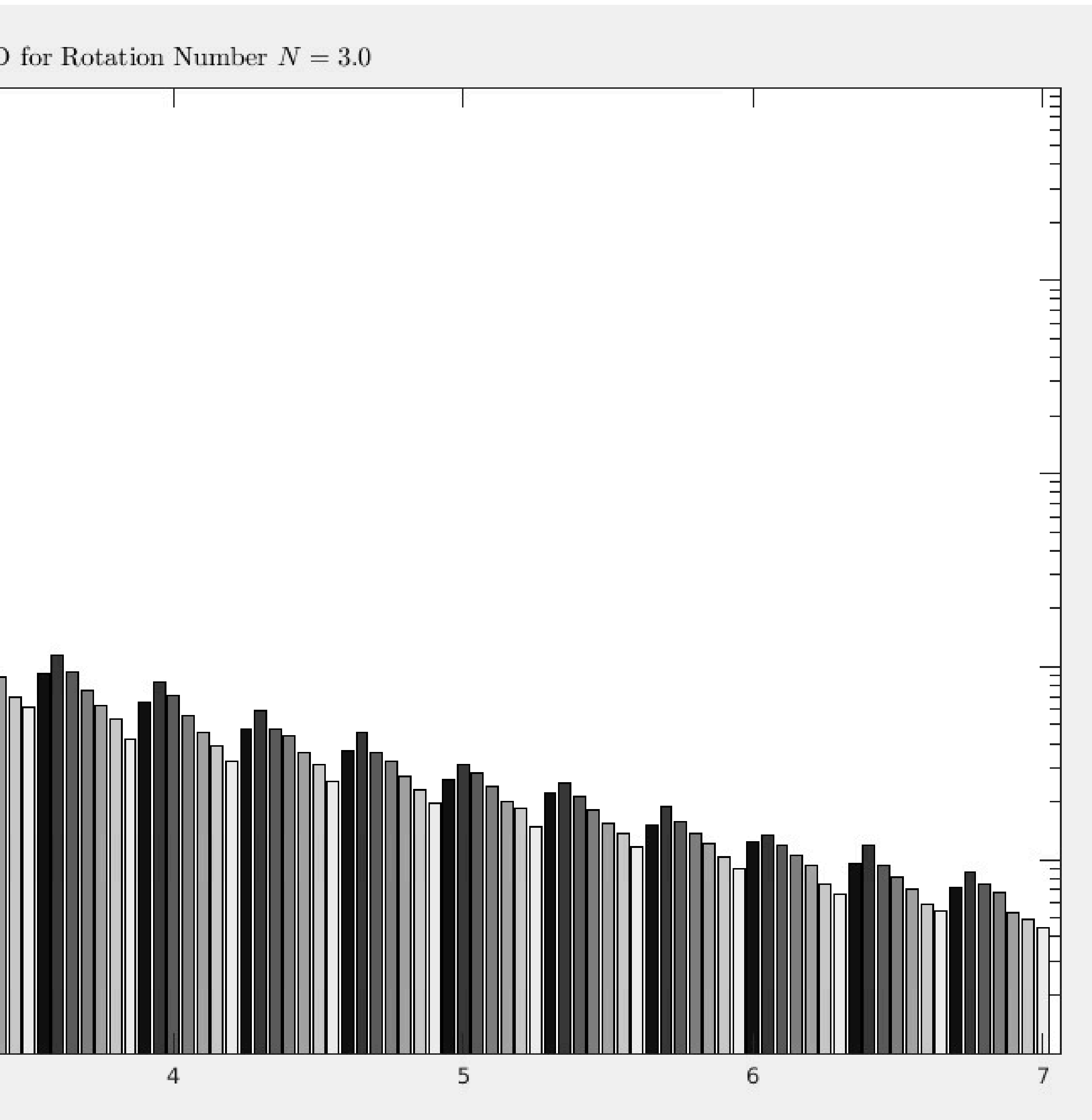

5.2. A

nalysis

6. Recon

struction

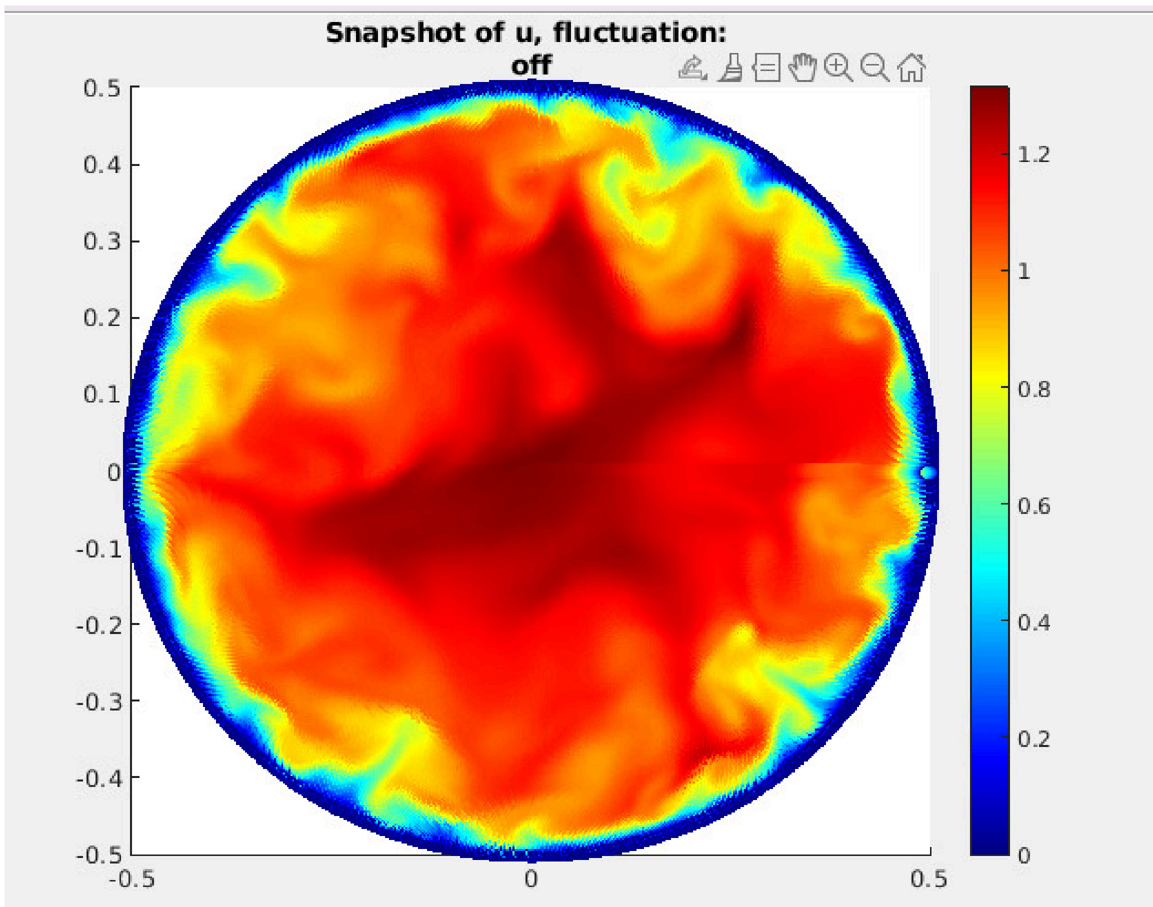
Snapshot of u, fluctuation:
off
0.5
0.4
0.3
0.2
0.1
0
-0.1
-0.2
-0.3
-0.4
-0.5
-0.5
0
0.5
1.2
1
0.8
0.6
0.4
0.2
0

nstruction

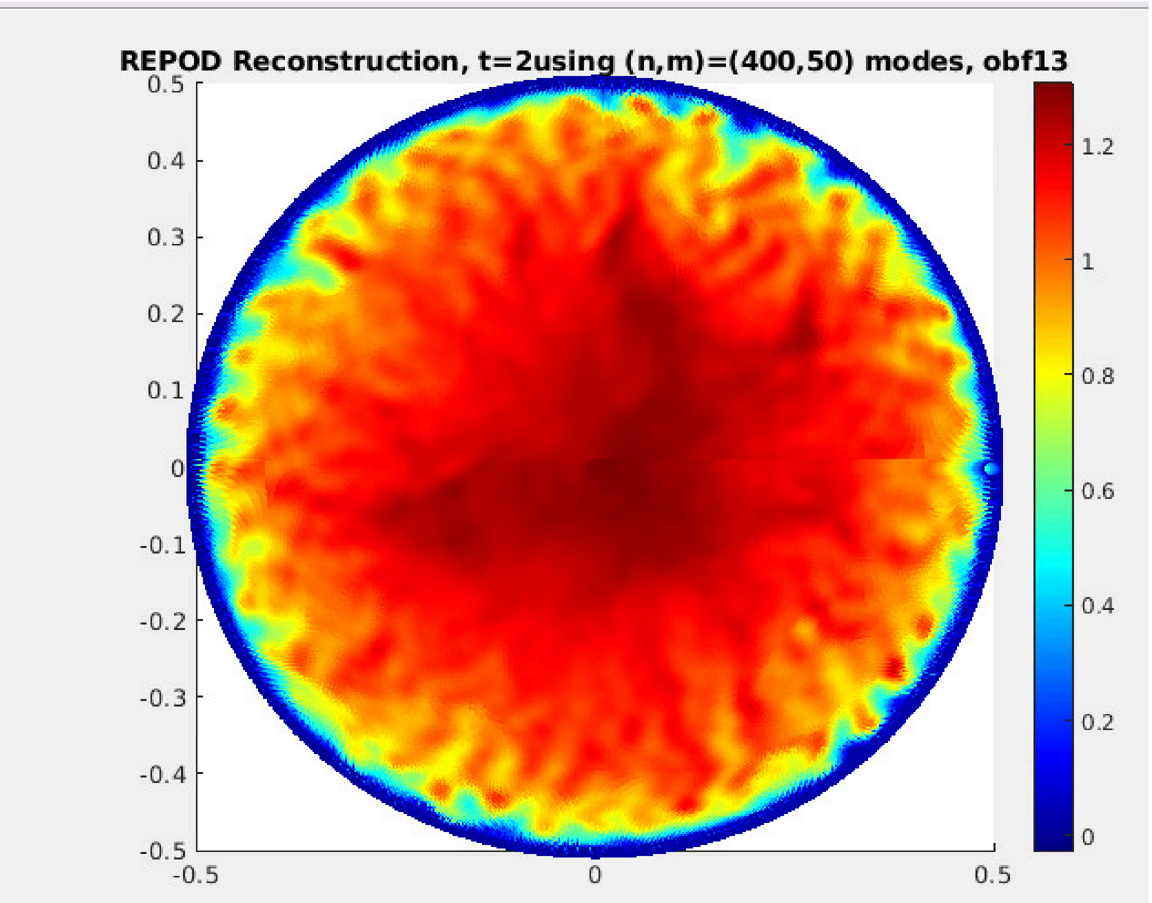

REPOD Reconstruction, t=2using (n,m)=(400,50) modes, obf13
0.5
0.4
0.3
0.2
0.1
0
-0.1
-0.2
-0.3
-0.4
-0.5
-0.5
0
0.5
1.2
1
0.8
0.6
0.4
0.2
0